Molecular Disambiguation of Heart Rate Control by the Nucleus Ambiguus

Maira Jalil*[,1], Tatiana C. Coverdell*[,2], Veronica A. Gutierrez[1], Maisie E. Crook[1], Jiachen Shi[1], Daniel. S. Stornetta[2], Dana C. Schwalbe[1], Stephen B. G. Abbott[#,2], John N. Campbell[#,1]

** equally contributing first author*
 # equally contributing senior author

[1] Department of Biology, University of Virginia, Charlottesville, VA
[2] Department of Pharmacology, University of Virginia, Charlottesville, VA

Correspondence to:

John N. Campbell (lead contact)
Department of Biology, University of Virginia
485 McCormick Road, PO BOX 4000328, Charlottesville, VA 22904
e-mail: jnc4e@virginia.edu

and

Stephen B. G. Abbott
Department of Pharmacology, University of Virginia
1340 Jefferson Park Avenue, Charlottesville, VA 22908
e-mail: sba6t@virginia.edu

SUMMARY

The nucleus ambiguus (nAmb) provides parasympathetic control of cardiorespiratory functions as well as motor control of the upper airways and striated esophagus. A subset of nAmb neurons innervates the heart through the vagus nerve to control cardiac function at rest and during key autonomic reflexes such as the mammalian diving reflex. These cardiovagal nAmb neurons may be molecularly and anatomically distinct, but how they differ from other nAmb neurons in the adult brain remains unclear. We therefore classified adult mouse nAmb neurons

based on their genome-wide expression profiles, innervation of cardiac ganglia, and ability to control HR. Our integrated analysis of single-nucleus RNA-sequencing data predicted multiple molecular subtypes of nAmb neurons. Mapping the axon projections of one nAmb neuron subtype, *Npy2r*-expressing nAmb neurons, showed that they innervate cardiac ganglia. Optogenetically stimulating all nAmb vagal efferent neurons dramatically slowed HR to a similar extent as selectively stimulating *Npy2r*+ nAmb neurons, but not other subtypes of nAmb neurons. Finally, we trained mice to perform voluntary underwater diving, which we use to show *Npy2r*+ nAmb neurons are activated by the diving response, consistent with a cardiovagal function for this nAmb subtype. These results together reveal the molecular organization of nAmb neurons and its control of heart rate.

INTRODUCTION

The parasympathetic nervous system powerfully slows heart rate by signaling through the vagus nerve. This was famously demonstrated in the mid-19th century by the Weber brothers, who found that electrically stimulating the vagus nerve slowed, and in some cases stopped, the hearts of frogs and mammals (Fye, 2000; Weber, 1846). Research since has demonstrated that cardiovagal signaling decreases heart rate at rest and during autonomic reflexes such as the baroreflex, respiratory sinus arrhythmia, and the diving reflex (Coverdell et al., 2024; Dampney, 2016; Ottaviani and Macefield, 2022). The diving reflex, for instance, first described by Edmund Goodwyn in 1786 (Goodwyn, 1786; Vega, 2017), is one of the most robust and evolutionarily conserved of autonomic reflexes (Butler and Jones, 1997; Panneton, 2013; Panneton and Gan, 2020). It occurs when voluntary apnea and facial immersion combine to trigger a dramatic decrease in heart rate (bradycardia), likely to conserve oxygen stores during an underwater dive (Alboni et al., 2011). Cardiovagal neurons mediate bradycardia during the diving reflex (Richet, 1899), though the molecular identity of the neurons involved remains unknown (Panneton et al., 2014; Panneton and Gan, 2020).

Cardiovagal fibers originate primarily from two medullary regions, the nucleus ambiguus (nAmb) and the dorsal motor nucleus of the vagus (DMV) (Geis and Wurster, 1980b; Standish et al., 1994; Stuesse, 1982). Cardiovagal axons project through the vagus nerve to synapse on postganglionic parasympathetic neurons in cardiac ganglia (Cheng and Powley, 2000; Cheng et al., 1999). At these ganglionic synapses, cardiovagal release of acetylcholine (ACh) activates

cardiac neurons via α4β2 nicotinic ACh receptors (Li et al., 2009) while potentially suppressing sympathetic input to the same neurons (Levy, 1971). CVNs may release other signaling molecules as well – for instance, neuropeptides such as PACAP (gene, *Adcyap1*) to modulate cardiac neuron excitability (Calupca et al., 2000; Tompkins et al., 2007) vasoactive intestinal peptide (VIP; gene, *Vip*) to control coronary artery flow (Feliciano and Henning, 1998). In turn, cardiac neurons synapse on cardiomyocytes in the sinoatrial (SA) and atrioventricular (AV) nodes, where their release of acetylcholine on muscarinic acetylcholine receptors slows cardiomyocyte electrical conduction and consequently decreases heart rate, AV conduction, and ventricular contractility. Vagotomy or blocking muscarinic receptors increases heart rate, indicating that parasympathetic tone sets heart rate at rest (Harvey, 2012; Reed, 1925; Reed and Layman, 1930).

Previous studies suggest the nAmb plays a larger role than the DMV in setting heart rate at rest and during reflexes such as the diving reflex (Chen and Chai, 1976; Geis et al., 1981; Geis and Wurster, 1980a; McAllen and Spyer, 1976; Panneton et al., 2014; Thomas and Calaresu, 1974). However, the nAmb is a functionally heterogeneous region which, in addition to its cardiovagal neurons, also contains respiratory parasympathetic neurons and motor neurons for the upper airways and esophagus (Bieger and Hopkins, 1987; Coverdell et al., 2024; Fryscak et al., 1984; Holstege et al., 1983; Lawn, 1966). Recent findings have raised the possibility that the nAmb's functional roles are delegated to different molecular subtypes of nAmb neurons (Coverdell et al., 2024; Coverdell et al., 2022; Veerakumar et al., 2022). Yet, a comprehensive understanding of these molecular subtypes in the adult brain and their anatomical and functional differences is still lacking. We therefore used single-cell transcriptomics to define the nAmb's molecular and cellular organization and uncovered one subtype which innervates cardiac ganglia, robustly decreases heart rate upon activation, and is activated during voluntary underwater diving.

RESULTS

Molecular Classification of Nucleus Ambiguus Neurons

To classify molecular subtypes of nucleus ambiguus (nAmb) neurons in adult mice, we compared their genome-wide RNA expression using single-nuclei RNA sequencing (snRNA-seq). First, to enrich for nAmb neurons, we fluorescently labeled their cell nuclei based on

expression of the cholinergic marker gene, *Chat,* which encodes choline acetyltransferase (ChAT) and which all nAmb vagal efferents and few neighboring cells express (Coverdell et al., 2022) (Supplemental Figure 1A). Specifically, we crossed mice in which Cre recombinase is driven by the *Chat* gene (Chat-Cre) (Rossi et al., 2011), to mice which Cre-dependently express a nuclear-localized mCherry fluorescent protein (H2b-mCherry; “H2b-TRAP” mice). The resulting Chat-Cre::H2b-TRAP mice exhibited H2b-mCherry expression in all peripherally projecting nAmb neurons (Coverdell et al., 2022) (representative example in Supplemental Figure 1B). As a complementary approach, to avoid any cells labeled due to Chat-Cre expression only during development, we injected the nAmb of other adult Chat-Cre mice with an adeno-associated virus (AAV) that Cre-dependently expresses H2b-mCherry. We then isolated mCherry+ cell nuclei from dissected nAmb tissue samples, processed their poly-adenylated RNA into sequencing libraries, and sequenced them (Figure 1A).

Our initial dataset contained 3,490 nuclear transcriptomes (“cells”) (Supplemental Figure 1C). Filtering out low-quality transcriptomes and likely cell doublets left 3,461 cells for further analysis (Supplemental Figure 1D). Grouping the pass-filter cells by their expression of high-variance genes yielded 18 clusters (Figure 1A). All of these clusters had representation from each batch (Supplemental Figure 1E,F). To identify the nAmb neuron clusters, we plotted expression of positive marker genes associated with cholinergic and motor neurons (vAChT/*Slc18a3*, *Isl1*, *Chat*) and negative marker genes (*Slc32a1*, *Slc17a6*) which are expressed around but not in the nAmb (Anderson et al., 2016; Coverdell et al., 2022; Sherman et al., 2015; Tanaka et al., 2003) (Figure 1A). Based on our results, we annotated five clusters, containing 1,245 neurons in total, as nAmb neurons.

We further explored the molecular heterogeneity of nAmb neurons by separating the 1,245 nAmb neurons and re-clustering them apart from non-nAmb neurons. This resulted in six clusters of nAmb neurons (Figure 1B). We detected on average (+/- SD) 2,927 +/- 967 genes per neuron, based on 6,666 +/- 3,565 unique transcripts per neuron (Figure 1C) and analyzed the composition of each cluster by batch (Supplemental Figure G,H). Comparing the neuron clusters revealed many differentially expressed genes (examples shown in Figure 1D). We annotated the clusters according to candidate marker genes (Supplemental Figure 1L). Among these was the gene *Adcyap1*, which is enriched in clusters n2 and n3 and encodes pituitary adenylate cyclase activating polypeptide (PACAP), a neuropeptide found in cholinergic axons

innervating the heart in guinea pigs (Calupca et al., 2000). Partially overlapping with *Adcyap1* expression and enriched in cluster n3 was *Npy2r*, the gene for neuropeptide Y receptor Y2, which modulates vagal control of heart rate (Herring et al., 2008) and is also expressed in vagal sensory neurons that control heart rate (Herring et al., 2008; Smith-White et al., 2002). Thus, our snRNA-seq identifies six candidate subtypes of nAmb neurons and raises the possibility that *Npy2r*+ nAmb neurons control heart rate.

Integrated Analysis Predicts Functional Identities of Nucleus Ambiguus Neuron Subtypes

We compared our nAmb neuron subtypes to those defined in two recent single-cell RNA-seq studies. One study, Coverdell et al., 2022, found three neuron subtypes among 141 adult mouse nAmb neurons: Crhr2^{nAmb} neurons, which control esophageal motor function; Vipr2^{nAmb} neurons, which innervate the pharynx and larynx; and Adcyap1^{nAmb} neurons, whose anatomy and function were unknown (Coverdell et al., 2022). Another study, Veerakumar et al. 2022, identified three subtypes from 203 neonatal mouse nAmb neurons innervating the larynx or heart: ACP neurons and ACV neurons, which can alter cardiopulmonary and cardiovascular function, respectively, and larynx-projecting neurons (Veerakumar et al., 2022). Plotting expression of subtype marker genes from these previously published studies by our nAmb neuron clusters suggests that our clusters n1, n2, and n3 may be cardiovagal neurons, whereas clusters n4, n5, and n6 may be motor neurons (Figure 2A).

To compare nAmb neuron subtypes more systematically across studies, we mapped single-cell transcriptomes from the Coverdell et al. and Veerakumar et al. studies onto our nAmb neuron clusters using reference query mapping. This method projects query cells onto reference cell clusters, without altering the reference data structure (Hao et al., 2021). Interestingly, while the Coverdell et al. cell clusters largely mapped to different reference cell clusters (Supplemental Figure 2A) as expected, the Veerakumar et al. cells subdivided among the same three reference clusters (Supplemental Figure 2B). This was surprising, since, for instance, the larynx-projecting subtypes in Coverdell et al. (Vipr2^{nAmb} neurons) and Veerakumar *et al.* (laryngeal neurons) mapped to different reference cell clusters. When we assessed the confidence of cell mapping, most Coverdell *et al.* cells mapped with high confidence (>0.8; Supplemental figure 2C) whereas most Veerakumar *et al.* cells mapped with lower confidence (<0.6; Supplemental figure 2D). This suggests that the adult nAmb neurons in Coverdell *et al*.

are more like the adult nAmb neurons in our dataset than are the neonatal nAmb neurons in Veerakumar *et al*., potentially due to developmental differences in gene expression. In line with this possibility, the larynx-projecting neurons of Veerakumar *et al*. but not in those of Coverdell et al. (Supplemental Figure 2E-F) expressed the gene *Adcyap1*, consistent with the broader expression of *Adcyap1* in the developing brain (Shuto et al., 1996). Thus, the ability to match neonatal and adult nAmb neurons using the reference query approach may be limited by their differences in gene expression.

Another method for relating cell types or states across studies is integrated clustering. Integrated clustering uses matching pairs of cells across datasets, referred to as anchors, to guide transformation of the datasets for joint analysis (Figure 2B) (Butler et al., 2018). Unlike reference query mapping, which transfers the reference data structure onto the query dataset, integration method learns the joint structure of datasets using canonical correlation analysis. Integrating our dataset with that of Coverdell et al. yielded six molecularly distinct clusters (Figure 2C). The Adcyap1^{nAmb} neurons from Coverdell et al. divided among integrated clusters cj1, cj2, and cj3, where they joined neurons from our n1.Kcnmb2, n2.Npy2r, and n3.Vip clusters, respectively (Figure 2D). This suggests that the Coverdell et al. Adcyap1^{nAmb} neurons correspond to the n1.Kcnmb2, n2.Npy2r, and n3.Vip neurons in the present study, consistent with the results of our reference query mapping. Similarly, most cells of the Coverdell *et al.* Crhr2^{nAmb} cluster and our n4.Pax2 cluster integrated into a single cluster, cj4, suggesting their similarity. Lastly, most Coverdell et al. Vipr2^{nAmb} neurons integrated with either our n5.Uts2 and n6.Stk32a clusters (Figure 2D), suggesting that n5.Uts2 and n6.Stk32a may represent subtypes of Vipr2^{nAmb} neurons, consistent with both of these clusters expressing the *Vipr2* gene (Figure 2A). Overall, the results of our integrated analysis relate the nAmb neuron clusters of Coverdell et al. with those of the present study.

We then used integration to compare the neonatal nAmb neurons of the Veerakumar et al. study with the adult nAmb neurons of the present study (Figure 2E). Interestingly, most Veerakumar *et al.* ACP (ambiguus cardiopulmonary) neurons integrated with most of our n1.Kcnmb2 neurons into cluster vj2 (Figure 2F). This suggests that our n1.Kcnmb2 neurons may be ACP neurons, consistent with their specific expression of the ACP marker genes *Trhr* and *Sema3d* (Figure 2A). Similarly, most Veerkumar *et al.* ACV (ambiguus cardiovascular) neurons integrated with our n3.Npy2r neurons into cluster vj4 (Figure 2F), consistent with

n3.Npy2r neurons being ACV neurons and their enriched expression of ACV marker genes, *Bche*, *Sstr2*, and *Lepr* (Figure 2A). However, unexpectedly, most Veerakumar et al. larynx-projecting neurons and our n5.Uts2 neurons also integrated into the same cluster (vj4) as the ACV and n3.Npy2r neurons (Figure 2F). This result raised questions about whether dataset integration could overcome the extent of differences between the neonatal nAmb neurons of the Veerakumar et al. study and the adult nAmb neurons of the current study. To investigate these differences, we compared gene expression between the Veerakumar et al. neurons and the corresponding clusters of the current study. We identified 2,229 genes which differed significantly between the two datasets (Figure 2G). Interestingly, many of these genes were exclusively detected in either Veerakumar *et al*. or the present study, though were broadly different across all cells, not just specific clusters (Figure 2H). Whether these differences in gene detection are due to the differences in mouse age between the studies, or other methodological differences, is unclear.

Partially Overlapping Populations of Nucleus Ambiguus Neurons Express Npy2r *and* Adcyap1

Given the likelihood that cardiovagal nAmb neurons express *Npy2r* and *Adcyap1*, we mapped the transcripts of these genes in the adult mouse nAmb using RNA fluorescence *in situ* hybridization (FISH). First, to label nAmb vagal efferent neurons, we intraperitoneally injected adult C57BL6/j mice with the retrograde tracer Fluorogold (Merchenthaler, 1991; Schmued and Fallon, 1986). We then performed RNA FISH for *Adcyap1*, *Npy2r*, and *Chat* transcripts in coronal sections and imaged them throughout the nAmb's compact, semi-compact, and loose subregions. We observed *Npy2r*+ nAmb vagal efferent neurons scattered throughout these subregions (representative images in Figure 3A), consistent with the known anatomical distribution of cardiovagal nAmb neurons (Geis et al., 1981; Kalia, 1981; Stuesse, 1982; Veerakumar et al., 2022). On the other hand, *Adcyap1*+ nAmb vagal efferent neurons resided in the compact and semi-compact, but not loose, nAmb, suggesting a slightly different anatomical distribution than *Npy2r*+ nAmb neurons. Quantifying nAmb neurons expressing *Adcyap1* and/or *Npy2r* revealed a partially overlapping distribution. Specifically, 4% of nAmb neurons expressed both *Npy2r* and *Adcyap1*, 3% expressed *Npy2r* but not *Adcyap1*, and <1% expressed *Adcyap1* but not *Npy2r* (Figure 3 A,B). Thus, a small minority of nAmb vagal efferent neurons express both *Adcyap1* and *Npy2r*. Of note, the 8% of nAmb neurons expressing *Adcyap1* and/or *Npy2r*, extrapolated for the total number of adult mouse nAmb neurons (Sturrock, 1990), would be

approximately 47 neurons per nAmb, slightly below previous estimates of retrogradely-labeled cardiovagal nAmb neurons in neonatal mice (50-60 neurons) (Veerakumar et al., 2022).

Npy2r *and* Adycap1 *Expressing Nucleus Ambiguus Neurons Innervate Cardiac Ganglia*

To determine whether *Npy2r*-expressing nAmb neurons (Npy2r^{nAmb}) and *Adcyap1*-expressing nAmb neurons (Adcyap1^{nAmb}) innervate the heart, we performed subtype-specific anterograde tracing with an AAV that Cre-dependently expresses tdTomato (AAV9-DIO-tdTomato). We first confirmed the Cre dependency of AAV9-DIO-tdTomato by injecting it into the nAmb of adult C57BL6/j mice. We failed to observe tdTomato immunofluorescence three weeks later at the injection sites, confirming the Cre-dependency of this AAV (n=3 mice; Supplemental Figure 3A). Next, to target this AAV to Npy2r^{nAmb} and Adcyap1^{nAmb} neurons, we obtained Npy2r-Cre and Adcyap1-Cre mice. We validated the specificity and sensitivity of Cre expression in these mice by co-localizing driver gene transcripts (i.e., *Npy2r* or *Adcyap1*) with Cre transcripts by RNA FISH in the nAmb. In Npy2r-Cre mice, 92% (145 of 157) *Npy2r* mRNA+ neurons were also *Cre* mRNA+, and 100% (145 of 145) of *Cre* mRNA+ cells were also *Npy2r* mRNA+ (n=3 mice). In Adcyap1-Cre mice, 89% (41 of 46) *Adcyap1* mRNA+ neurons were Cre+ and 100% (41 of 41) of *Cre* mRNA+ cells were also *Adcyap1* mRNA+ (n=2 mice; Supplemental Figure 3B). These results validate the specificity of AAV9-DIO-tdTomato, Npy2r-Cre, and Adcyap1-Cre mice for genetically targeting Npy2r^{nAmb} neurons and Adcyap1^{nAmb} neurons.

To fluorescently label Npy2r^{nAmb} and Adcyap1^{nAmb} axons for anterograde tracing, we injected the nAmb of Npy2r-Cre and Adcyap1-Cre mice with AAV-DIO-tdTomato (Figure 4A). As a positive control, we also injected the nAmb of Chat-Cre mice, which express Cre activity in all nAmb vagal efferent neurons (Coverdell et al., 2022) (Chat^{nAmb} neurons). After waiting at least three weeks for AAV transgene expression, we observed tdTomato immunofluorescence in a subset of nAmb neurons, identified based on their immunofluorescence of the cholinergic marker ChAT (Figure 4B). While some neurons outside the nAmb in Npy2r-Cre mice and Adcyap1-Cre mice were also tdTomato+, none were ChAT+ (Figure 4B), indicating that they were not vagal efferents and so would not confound our analysis. Importantly, we observed no tdTomato+ neurons in the dorsal motor nucleus of the vagus (DMV), another source of heart innervation (Supplemental Figure 3C) (Nosaka et al., 1979; Stuesse, 1982). To determine whether Npy2r^{nAmb} and Adcyap1^{nAmb} neurons innervate the heart, we then imaged immunofluorescence

of tdTomato and the neuronal marker protein PGP9.5 in cardiac tissue from the same mice. We observed fibers immunofluorescent for both tdTomato and PGP9.5 innervating cardiac ganglia in all Npy2r-Cre, Adcyap1-Cre and Chat-Cre mice (Figure 4C). These results indicate that Npy2r^{nAmb} neurons and Adcyap1^{nAmb} neurons innervate cardiac ganglia.

Activating Npy2r-*Expressing Nucleus Ambiguus Neurons Reduces Heart Rate*

Since Npy2r^{nAmb} neurons innervate cardiac ganglia, their activity could affect heart rate. To investigate this possibility, we used intersectional optogenetics to activate nAmb neuron subtypes in mice while recording electrocardiography (ECG). To intersectionally target Npy2r^{nAmb} neurons, we bred Npy2r-Cre mice (Chang et al., 2015) to Chat-Flp mice (Coverdell et al., 2022), and then crossed their Npy2r-Cre;Chat-Flp offspring to a transgenic reporter line which Cre- and Flp-dependently expresses a calcium-translocating channelrhodopsin (CaTCh; Figure 5A) (Madisen et al., 2015). In the resulting Npy2r-Cre;Chat-Flp;CaTCh offspring, we validated the specificity of CaTCh-eYFP expression by co-localizing its immunofluorescence with *Cre* and *Flp* RNA by FISH (64 of 74 eYFP+ cells, or 86%, contained both *Cre* and *Flp* RNA, 9 contained only *Cre* RNA, and 1 contained neither *Cre* nor *Flp* RNA; n=3 mice). As positive and negative controls, respectively, we also included groups of mice expressing CaTCh in all nAmb efferent vagal neurons (Chat^{nAmb} neurons; Chat-Cre;Phox2b-Flp;CaTCh mice), validated previously (Coverdell et al., 2022), and CaTCh mice which lacked any Cre or Flp expression (CaTCh-negative controls) (Figure 5A).

Photostimulating Npy2r^{nAmb} neurons in freely-behaving conditions produced severe bradycardia with rapid onset and offset kinetics (Figure 5B,E-G), whereas HR was unchanged during photostimulation in control mice (Figure 5C,E-G). Photostimulating Chat^{nAmb} neurons also produced bradycardia with rapid kinetics (Figure 5D,E-G), consistent with the co-expression of *Chat* and *Phox2b* in cardiovagal neurons. On the other hand, we have previously shown that photostimulating Crhr2^{nAmb} neurons (Crhr2-Cre;Chat-Flp;CaTCh mice) and Vipr2^{nAmb} neurons (Vipr2-Cre;Chat-Flp;CaTCh mice), which innervate the esophagus and upper airways, does not affect heart rate (Figure 5F; Crhr2^{nAmb} and Vipr2^{nAmb} data from ref. (Coverdell et al., 2022)). Strikingly, photostimulating Npy2r^{nAmb} and Chat^{nAmb} neurons produced a comparable reduction in HR (ΔHR during 10 Hz stimulation; –277 ± 45 bpm vs. –257 ± 67 bpm, respectively) (Figure 5F), indicating that Npy2r^{nAmb} neuron activation affects HR to a similar extent as activating all

cardiovagal neurons. Moreover, the HR effect of photostimulating Npy2r^{nAmb} neurons was stimulus-frequency dependent (Figure 5G), persisted under isoflurane anesthesia (Figure 5H,I), and was blocked by systemic blockade of muscarinic receptors with atropine (Figure 5J,K). Our results demonstrate that, unlike Crhr2^{nAmb} neurons and Vipr2^{nAmb} neurons, activating Npy2r^{nAmb} neurons decreases heart rate through peripheral muscarinic signaling and to a similar extent as activating nAmb neurons non-specifically.

Voluntary Underwater Diving Activates Npy2r-*Expressing Nucleus Ambiguus Neurons*

Underwater submersion stimulates the diving response in most mammals, which involves a powerful bradycardia driven by activation of cardiovagal neurons (Panneton, 2013). Based on the potent bradycardic response to stimulation of Npy2r^{nAmb} neurons, we hypothesized that these cells would be activated by the diving response. We tested this hypothesis by evaluating expression of the immediate early gene and neuronal activation marker, *Fos*, in nAmb neurons following voluntary diving. To achieve this, we trained mice to voluntarily dive up to 20 cm underwater to reach an escape platform (Figure 6 A,C). We first validated that this model evokes a diving response by measuring EKG using radio-telemetry implants (Figure 6A,B). Heart rate decreased markedly upon initiation of the dive and remained low while underwater before recovering to baseline following a brief overshoot after the mice resurfaced (Figure 6A,B), consistent with previous descriptions. We then performed a session of repeated diving for up to 30 mins to robustly activate the diving response before perfusing mice for histology. Controls were handled and allowed to explore the test chamber emptied of water but did not perform any dives (Figure 6C). In mice that performed voluntary diving, we observed a 174% increase in the proportion of Npy2r^{nAmb} neurons that expressed *Fos* (dive vs. control, 44.5 ± 5.5% vs. 16.3 ± 4.3% Npy2r^{nAmb} neurons expressing Fos, unpaired t-test, t=3.915, df=11, p=0.0024) (Figure 6D,F,E). Cell counts for total Npy2r^{nAmb} neurons were similar between cases (42 ± 6 vs. 45 ± 6 cells per unilateral nAmb in a 1 in 3 series, unpaired t-test, t=0.3679, df=11, p=0.72), and a similar proportion of FG cells expressed Npy2r between cases (17.6 ± 1.6 vs. 20.6 ± 3.5% of all FG cells expressed *Npy2r*, unpaired t-test, t=0.7933, df=11, p=0.44). These data indicate that Npy2r^{nAmb} neurons are activated during voluntary diving, consistent with these cells being functionally important for the parasympathetic regulation of the heart.

DISCUSSION

This study identified cardiovagal nAmb neurons based on their molecular, anatomical, and functional features. Transcriptomic profiling and clustering analysis of 1,245 nAmb neurons identified six molecularly distinct subtypes. RNA fluorescence *in situ* hybridization (RNA FISH) and anterograde tracing showed that *Adcyap1*+ nAmb neurons and *Npy2r*+ nAmb neurons are rare and partially overlapping populations of nAmb neurons which innervate cardiac ganglia. Activating *Npy2r*+ nAmb neurons with intersectional optogenetics decreased heart rate to a similar extent as activating all nAmb neurons. Finally, voluntary underwater diving significantly increased the percentage of *Fos*-expressing *Npy2r*+ nAmb neurons, indicating that these neurons are activated during the diving reflex. Overall, our study identifies *Npy2r*+ nAmb neurons as molecular subtype which innervates cardiac ganglia, decreases heart rate upon activation, and is activated during the diving reflex.

Our study provides a more comprehensive understanding of the molecular subtypes of nAmb neurons than previously known. Two studies previously used single-cell RNA-seq to molecularly classify subtypes of nAmb neurons. For instance, Coverdell et al. (2022), identified three subtypes from 145 *Chat*-expressing nAmb neurons of adult mice (Coverdell et al., 2022). Another study, Veerakumar et al. (2023), classified three subtypes of nAmb neurons from 203 heart- or larynx-projecting nAmb neurons of neonatal mice (Veerakumar et al., 2022). However, each of these previous studies contained far fewer neurons than the nearly 1,200 found bilaterally in adult mouse nAmb (Sturrock, 1990) and so may have underestimated the diversity of nAmb neurons. Our present study identified six molecular subtypes from 1,245 *Chat*-expressing nAmb neurons, doubling the number of previously known subtypes. However, our results do not rule out the possible existence of rare subtypes of nAmb neurons. In addition, whether there are differences in the subtypes present in each hemisphere of the nAmb remains an open question, especially since the right vagus controls heart rate more strongly than the left, e.g., (Muppidi et al., 2011).

Our present study provides a finer resolution of nAmb neuron subtypes than previously known. For instance, a previous study by our group identified three subtypes of nAmb neurons (Coverdell et al., 2024), which our integrated analysis now resolves as six subtypes. One subtype identified in our previous dataset, Adcyap1^{nAmb} neurons, comprises three subtypes in the combined dataset: Kcnmb2^{nAmb} , Vip^{nAmb} , and Npy2r^{nAmb} neurons. Another previously

defined population, Vipr2^{nAmb} neurons, divides into two subtypes, Uts2^{nAmb} and Stk32a^{nAmb}, in the present study. Since Vipr2^{nAmb} neurons innervate the pharynx and larynx, future studies could investigate whether the Uts2^{nAmb} and Stk32a^{nAmb} subtypes separately innervate these two cervical regions. Interestingly, *Uts2* and *Uts2b* expression mark vocal control regions in birds (Bell et al., 2019) and are enriched in the n5.Uts2 subtype of mouse nAmb neurons in the current study, raising the possibility that this subtype innervates the larynx to control vocalization.

Integrating our dataset with that of another previous study also sheds light on the functional identities of our nAmb neuron subtypes. Veerakumar and colleagues identified three functional subtypes of nAmb neurons: cardiopulmonary nAmb neurons (ACP), which cause bradycardia and bronchoconstriction; cardiovascular nAmb neurons (ACV), which cause bradycardia without bronchoconstriction; and larynx-projecting nAmb neurons (Veerakumar et al., 2022). Integrating the single-cell transcriptomic data from the current study and Veerakumar et al. suggests that Kcnmb2^{nAmb} neurons and Npy2r^{nAmb} neurons of the current study may correspond to ACP neurons and ACV neurons, respectively, of the Veerakumar study. However, differences in gene expression between the datasets, potentially related to age differences in mice between studies, limit the ability to compare nAmb neuron subtypes between the Veerakumar et al. study and the present one. Also, while Veerakumar et al. did not detect an increase in Fos expression in ACV neurons after nasal immersion in anesthetized mice, suggesting a lack of involvement in the diving reflex. In contrast, our results show that Fos expression increases in Npy2r^{nAmb} neurons in response to voluntary underwater diving. If Npy2r^{nAmb} neurons are ACV neurons, then it is possible they are activated differently by nasal immersion in the anesthetized state than by voluntary underwater diving.

The molecular profile of Npy2r^{nAmb} neurons raises hypotheses about signaling pathways through which the vagus nerve controls heart rate. For instance, the neuronal nitric oxide synthase, *Nos1*, mediates vagal control of heart rate (Choate et al., 2001). Our study found enriched expression of *Nos1* in the Npy2r^{nAmb} neurons relative to the other nAmb neurons, raising the possibility that Npy2r^{nAmb} neurons release nitric oxide onto cardiac neurons to control heart rate. In addition, Npy2r^{nAmb} neurons also selectively express other genes encoding signaling proteins that affect heart rate, including *Adcyap1*/PACAP (Chang et al., 2005; Hirose et al., 1997), *Trpc5* (Lau et al., 2016), and *Calm1*/Calmodulin (Nyegaard et al., 2012). Future studies using

conditional knockouts could investigate whether these genes control heart rate through their action in Npy2r^{nAmb} neurons.

ACKNOWLEDGMENTS

We gratefully acknowledge Patrice G. Guyenet, Ruth Stornetta, and Steven J. Swoap for thoughtful discussion and feedback on the experimental design; Bradford B. Lowell for the Chat-Flp mouse line; Stephen D. Liberles for the Npy2r-Cre mouse line; Patrice G. Guyenet and Hui Zong for co-acquisition of pilot funding; and Moon Snyder, Natalie Schiavone, and Virginia Owen Trinkle for technical support. We also acknowledge the valuable assistance of these UVA core facilities: the Robert M. Berne Cardiovascular Research Center Histology Core; the Biology Department Genomics Core; the Genome Analysis and Technology Core (RRID:SCR_018883); and the Flow Cytometry Core Facility. Funding was provided by a University of Virginia 3 Cavaliers award to J.N.C., Patrice G. Guyenet, and Hui Zong; NIH R01 HL148004 to SBGA; NIH T32 GM007055 and NIH F31 HL158187 to TCC; and a Pathway to Stop Diabetes Initiator Award 1-18-INI-14 and NIH R01 HL153916 to JNC.

AUTHOR CONTRIBUTIONS

MJ, TCC, VAG, SBGA, and JNC designed the experiments. MJ, JNC, and TCC generated the 10X sequencing data and MJ analyzed it. TCC and SBGA performed RNA FISH studies for Figure 2 and Figure 5 respectively. MEC performed surgeries for the anterograde tracing studies. MJ performed cardiac immunofluorescence. TCC and SBGA performed the optogenetic studies. TCC validated the mouse lines. JS and TCC imaged tissue to assess fiber placements. VAG developed the diving reflex assay and with MEC generated and analyzed diving reflex data. MJ, TCC, VAG, SBGA, and JNC prepared the figures. MJ, TCC, SBGA, and JNC wrote the manuscript, with input from all the authors.

DECLARATION OF INTERESTS

The authors declare no competing interests.

METHODS

Resource Availability

The accession number for the raw and processed sNuc-seq data and metadata reported in this paper is GEO accession number ######. A user-friendly interface for visualizing and exploring the sNuc-seq data is available at the Broad Institute Single Cell Portal at ######. The code used for processing, clustering, and visualizing the clustered single-nuclei RNA-seq data is publicly available through Zenodo at ######. Any additional information required to reanalyze the data reported in this paper is available from the lead contact upon request.

Lead Contact

The lead contact is John Campbell, jnc4e@virginia.edu.

Experimental Model and Subject Details

All animal care and experimental procedures were approved in advance by the University of Virginia Institutional Animal Care and Use Committee. The single-cell RNA-seq experiments used 28 - 35 week old male and female B6;129S6-*Chat*$^{tm2(cre)Lowl}$/J mice ("Chat-Cre"; (Jackson Laboratories, JAX, strain # 028861) (Rossi et al., 2011) crossed to a nuclear reporter mouse line B6.Cg-*Gt(ROSA)26Sortm1(CAG-HIST1H2BJ/mCherry,-EGFP/Rpl10a)Evdr*/J ("H2b-TRAP"; JAX strain #029789) (Roh et al., 2017). The fluorescent *in situ* hybridization experiments used C57BL/6J mice from the Jackson Laboratory (JAX, strain # 000664). The following mouse lines were used for optogenetic studies: Chat-Cre; B6;D2-Tg(Phox2b-flpo)3276Grds/J ("Phox2b-Flp"; JAX, strain # 22407) (Hirsch et al., 2013); B6.Cg-*Gt(ROSA)26Sortm80.1(CAG-COP4*L132C/EYFP)Hze*/J ("CaTCh"; JAX, strain # 025109) (Madisen et al., 2015); B6.Cg-*Adcyap1tm1.1(cre)Hze*/ZakJ ("Adcyap1-Cre"; JAX, strain # 030155) (Harris et al., 2014); *Npy2rtm1.1(cre)Lbrl*/RcngJ ("Npy2r-Cre"; Stephen Liberles, Harvard Medical School, Howard Hughes Medical Institute) (Chang et al., 2015); and Chat$^{em1(flp)Lowl}$ ("Chat-Flp"; Bradford Lowell, Beth Israel Deaconess Medical Center, Harvard Medical School) (Coverdell et al., 2022). The anterograde tracing experiments used Chat-Cre, Npy2r-Cre, Adcyap1-Cre, and C57BL/6J mice. Unless otherwise specified, all experiments used adult mice with approximately equal numbers

of male and female mice. Mice were housed at 22-24 °C with a 12 hour light:12 hour dark cycle and unlimited access to standard mouse chow and water.

Fluorescently Labeling Nucleus Ambiguus Neurons

To label the nAmb *Chat*+ neurons, two approaches were used. One approach crossed Chat-Cre mice with the H2b-TRAP transgenic mouse line, which Cre-dependently labels cells with mCherry-tagged histone 2B protein (H2b-mCherry) and eGFP-tagged ribosomal L10 protein. Preliminary transcriptomic analysis failed to detect *Chat* expression in many Chat-Cre;H2b-TRAP-labeled cells (Figure 1A, far right panel), consistent with developmental Chat-Cre activity in brain regions around the nAmb. Therefore, a second labeling approach was used to enrich the sample with nAmb *Chat*+ neurons. Specifically, the ventrolateral medulla of eight male and female Chat-Cre mice were injected with a Cre-dependent reporter virus, AAV9-Syn1-FLEX-H2b-mCherry (Vigene Biosciences, 3.94 x 10^{13} GC/mL) on the right side of nAmb, four weeks prior to tissue collection (see below for details on surgery).

Single-Nuclei RNA-Sequencing

Tissue samples of nAmb were collected after rapid decapitation of the mice to avoid stress- and anesthesia-related changes in nuclear mRNA. Brains were immediately extracted, chilled in slush, and sectioned coronally at 1 mm intervals through the nAmb's full rostral-caudal extent (Bregma −6.5 mm to −8.0 mm). The brain sections were immersed in ice-cold RNAprotect (Qiagen, catalog # 76106) to preserve RNA during microdissection and storage. After at least 30 min in RNAprotect, the nAmb was visualized under a fluorescence stereomicroscope (Zeiss Discovery V8), dissected, and stored in RNAprotect overnight at 4 °C. On the next day, nAmb tissue was homogenized and purified by density-gradient centrifugation into a single-nuclei suspension as previously described (Habib et al., 2016; Todd et al., 2020). The single-nuclei suspension was sorted by FACS using 80 nm nozzle to collect H2b-mCherry+ nuclei in a 2 mL microcentrifuge tube. The sample was then processed using 10X Genomics Chromium Next GEM Automated Single Cell 3' cDNA Kit v3.1 as previously described (Zheng et al., 2017). 10X cDNA libraries were sequenced on an Illumina Next-Seq 550 with high-output, 75-cycle v2.5 kits. Sequencing reads were demultiplexed by bcl2fastq2 v2.20.0 (Illumina) and aligned to the

mouse genome mm10-2020-A with 10X Genomics Cell Ranger software pipeline 5.0.0 using the include-intron function (Supplemental Figure 1C).

Gene expression matrices output from the 10X Cell Ranger pipeline were input to Seurat v4.3.0 in R (version 4.1.2) for data analysis. Genes detected in fewer than three cells, cells with fewer than 200 genes, and cells with more than 2% of reads mapping to mitochondrial genes (%mt) were filtered out. Pass-filter data were then merged across batches and integrated to correct for technical differences including batch effects (Stuart et al., 2019). The following steps were then performed: log-normalization of the data; selection of the 2,000 highest-variance genes using Seurat's FindVariableFeatures() function; batch integration using the IntegrateData() function in Seurat; scaling of gene expression values; Principal Component Analysis (PCA) for linear reduction of the dimensionality of data; cell clustering using Louvain algorithm, based on Euclidean distance in the PCA space comprising the first 13 PCs and with a resolution of 1; and non-linear dimensionality reduction by Uniform Manifold Approximation and Projection (UMAP) for visualization in two dimensions (Armstrong et al., 2021).

To enrich our analysis with nucleus ambiguus neurons, we included neuron clusters expressing *Slc18a3, Isl1* and *Chat* and excluded neuron clusters expressing *Slc32a1* and *Slc17a6* (Figure 1A). After removing non-nAmb neurons, the remaining neurons were re-clustered, including the steps of feature selection, PCA, clustering with the top 17 PCs and resolution setting of 0.25. Integration of all nAmb neurons was performed again with 12 PCs at 0.25 resolution. Cluster relatedness in PCA space was illustrated with dendrograms using Seurat's BuildClusterTree() function. Differentially expressed genes in each cluster were identified using Seurat's FindAllMarkers() function with the Wilcoxon Rank Sum test and p values Bonferroni-adjusted for multiple comparisons. The results were filtered to only include positive marker genes expressed in a minimum fraction of 0.25 cells with log2-fold change threshold of 0.25. Candidate marker genes were then selected based on their expression specificity in each cluster.

RNA Fluorescence In Situ Hybridization (FISH)

RNA FISH experiments were performed on brain tissue from mice, some of which received an intraperitoneal injection of 2% Fluorogold (Fluorochrome) to label nAmb vagal efferent neurons a minimum of 5 days prior to euthanasia. Mice were terminally anesthetized with ketamine (20

mg/kg) and xylazine (2 mg/kg) diluted in sterile saline, followed by transcardial perfusion with 0.9% saline plus heparin and 4% paraformaldehyde (Thomas Scientific). Brains were extracted and post-fixed in 4% paraformaldehyde for 24 hr at 4 °C. Following fixation, brains were sectioned coronally at 30 - 35 um thickness on a vibratome (VT-1000S, Leica). The day before FISH, the sections were rinsed in PBS and then mounted on precleaned Superfrost Plus microscope slides (Fisher, catalog # 12-550-15) and left to dry overnight. An ImmEdge Hydrophobic Barrier Pen was used to draw a barrier around the sections. The sections were then incubated in Protease IV in a HybEZ II Oven for 30 min at 40°C, followed by incubation with target probes (*Chat*, *Phox2b*, *Adcyap1*, *Npy2r*, *Phox2b, Cre,* and *Flp*) for 2 hr at 40 °C. Slides were then treated with AMP 1-3, HRP-C1, HRP-C2, HRP-C3, and HRP Blocker for 15-30 min at 40 °C, as previously described (Wang et al., 2012). FITC, Cy3, and Cy5 (Perkin Elmer) fluorophores were used for probe visualization. Fluorogold was imaged based on its native fluorescence. Images were taken using a confocal microscope (Zeiss LSM 800). The three levels of the nucleus ambiguus correspond to the following bregma levels: rostral or compact nAmb: -6.47 mm through -6.75 mm from bregma; intermediate or semi-compact nAmb: -6.83 mm through -7.10 mm from bregma; caudal or loose nAmb: -7.19 mm through -7.46 mm from bregma.

Virus Injections

Mice were anesthetized with ketamine (20 mg/kg) and xylazine (2 mg/kg) and positioned in a stereotaxic apparatus (Kopf). A pulled glass micropipette was used for stereotaxic injections of AAV-FLEX-tdTomato (Addgene plasmid # 28306; http://n2t.net/addgene:28306; RRID:Addgene_28306; a gift from Edward Boyden) or AAV-DIO-H2b-mCherry (Vigene Biosciences, 3.94 x 10^{13} GC/m) using the following stereotaxic coordinates for the nucleus ambiguus: anterior/posterior -2.1, -2.4, -2.7 mm, lateral/medial +/- 1.3 mm, and dorsal/ventral -5.8 mm, from lambda; and anterior/posterior -0.1 mm, lateral/medial +/- 1.3 mm, and dorsal/ventral -0.1, -1.3 mm, from the calamus scriptorus. Following local anesthetization with bupivacaine, the virus was injected (50 nL/injection, 3 injections on the right side) using a Nanoject III system. This injection strategy was designed to fully cover the nAmb and avoid DMV, but not to restrict viral infection to only nAmb neurons. The pipette was removed 5 minutes after injections, followed by wound closure with sutures or surgical wound glue

(Vetbond). Meloxicam SR (5 mg/kg; sustained release, SR) was injected subcutaneously for post-operative analgesia.

Tissue Histology and Immunofluorescence

Three to four weeks after AAV-FLEX-tdTomato injection, mice were deeply anesthetized with ketamine (20 mg/kg) and xylazine (2 mg/kg) diluted in sterile saline, then transcardially perfused with 0.9% saline plus heparin followed by 4% paraformaldehyde (PFA) (Thomas Scientific; CAS#30525-89-4). Brains and hearts were harvested and shaken in 4% paraformaldehyde overnight at room temperature for continued fixation. Brains were either sectioned on vibratome at 35 um or cryoprotected in 30% sucrose on a shaker at 4 °C overnight and then sectioned on freezing microtome at 35 um. Hearts were cryoprotected in 30% sucrose solution in 4 °C on a shaker for 2 days. Hearts were then cut with a 10 blade (Fine Science Tools, Catalog #10010-00) along the dorsal ventral axis and were then embedded in optimal cutting temperature (OCT) compound and sectioned on cryostat (Thermo Scientific CryoStar NX50) at 10 um intervals. Slide-mounted cardiac sections were then kept at –80 °C for long term storage.

For heart immunofluorescence, slides were removed from –80 °C and placed flat on a tray in a fume hood to dry at room temperature. A hydrophobic barrier was drawn to contain solutions on the slide, and the slides were left to air dry for 10 min. The slides were then placed in the pre-chilled Coplin jar containing acetone in –20 °C for 10 min. After 10 min, acetone was removed, and the slides dried in the fume hood for 10 min. A 0.1% Sudan Black solution dissolved in 70% ethanol was added for 20 min to reduce autofluorescence. Tissue was then washed three times for 5 min with PBS. 0.1% PBST was prepared by dissolving 100 uL of Triton-X100 (Sigma Life Sciences, catalog # 9036-19-5) in 100 ml 1X PBS (Fisher, catalog # 70-013-032). Chat-Cre and Npy2r-Cre heart tissues were incubated in a blocking buffer for an hour on a shaker at room temperature. The blocking buffer consisted of 5% donkey serum (Millipore Sigma, catalog # S30-100ML) in 0.1% PBST. Tissue was then incubated overnight at 4 °C on a shaker in primary antibodies against PGP9.5 (from rabbit; Abcam, catalog # EPR4118) and tdTomato (from goat; Arigo Biolaboratories, catalog # ARG55724) diluted 1:500 in 5% donkey blocking buffer. Due to import-related supply issues for the Arigo tdTomato antibody, a different antibody was used for the Adcyap1-Cre tissue. Adcyap1-Cre tissue was incubated in a solution of 10% donkey serum in 0.1% PBST for an hour at room temperature, then incubated in primary antibodies against

PGP 9.5 (from chicken; Thermo Fisher, catalog # PA1-46204; 1:1000 dilution) and RFP (from rabbit; Rockland, catalog # 600-401-379; 1:1000 dilution) diluted in 10% donkey blocking buffer.

For brain immunohistochemistry, tissue was rinsed in PBS three times for 5 minutes on a shaker at room temperature, followed by incubation in 5% blocking buffer (5% normal donkey serum + 0.1% PBST) for 1 hour at room temperature on the shaker. Brain sections were then incubated in primary antibody against ChAT (from goat; Sigma Aldrich, catalog # AB144P; 1:100 dilution).

After primary antibody incubation, heart and brain sections were then rinsed three times for 5 minutes in 0.1% PBST solution. Species-specific donkey secondary antibodies conjugated to Alexa Fluor 488, 568 or 647 were obtained from Abcam or Invitrogen and heart and brain sections were incubated in secondary antibodies (dilution 1:1000) for 2-4 hours on a shaker at room temperature. After three 5 minutes in PBS washes, the tissue was mounted on Superfrost Plus precleaned slides (Fisher; catalog # 12-550-15) followed by cover-slipping with Prolong Gold antifade mounting media (Cell Signaling Technology, catalog # 9071S) and sealed with nail polish.

Optogenetic Physiology

Mice with and without CaTCh expression in the nAmb were implanted with an optical fiber over the right nAmb. Optical fibers for central stimulation and headsets to record electrocardiogram (ECG) were implanted under anesthesia with ketamine (150 mg/kg) and dexmedetomidine (1 mg/kg). Depth of anesthesia was assessed by absence of the corneal and hind-paw withdrawal reflex. The body temperature was maintained at 37.2 ± 0.5 °C with a servo-controlled temperature pad (TC-1000; CWE). Following confirmation of anesthesia, mice were prepped for surgery, positioned in a stereotaxic headframe, and the local anesthetic, Bupivacaine (50 uL, 5 mg/mL), was injected at surgical sites. The tissue overlying the dorsal surface of the skull was retracted and the surface of the skull prepped for headset and optical fiber implants.

EKG headsets were constructed from 4-pin miniature connectors soldered to 2 lengths of Teflon-coated multi-strand stainless steel wire (AM-systems) for positive and negative leads and a stainless-steel screw implanted in the skull for the ground. The screw was implanted above

the frontal cortex and the leads were tunneled subcutaneously to opposing locations near the base of the ribcage. An optical fiber cannula constructed (200 um, 0.39NA fiber, Thorlabs) was implanted to stimulated cell bodies in the nucleus ambiguus neurons using the following coordinates from lambda: anterior/posterior: -2.1 mm, medial/lateral: +1.3 mm, dorsal/ventral: -5.0 mm for Crhr2-Cre;Chat-Flp;CaTCh mice. Fibers were only implanted on the right side of the brain. The same coordinates were used for Npy2r-Cre;Chat-Flp;CaTCh, Adcyap1-Cre;Phox2b-Flp;CaTCh, Vipr2-Cre;Chat-Flp;CaTCh mice, but at a 10 degree angle to access these neurons, which are found in the semi compact (intermediate) and loose (caudal) nAmb. The fiber and ECG headset was secured to the skull with dental cement and wounds were closed with sutures and surgical glue. Mice were given ketoprofen (5 mg/kg) for analgesia 3 days after surgery and allowed to recover for a minimum of 5 days before optogenetic physiology experiments.

To assess the cardiac effects of stimulating nucleus ambiguus neurons without anesthesia, mice were scruffed to connect the ECG head set to an amplifier and to connect a fiber optic cable to a laser. After 30 min to 1 hr of habituation to the recording set-up, stimulation was performed with a diode laser (473 nm; LaserGlow) controlled by Spike 2 software (Cambridge Electronic Design, UK). ECG (gain: 2K, band pass filter: 10-1000 Hz) signal was acquired (sampling rate: 1K) and heart rate calculated using Spike 2 software. Stimulation consisted of a 10 sec period of stimulation at 5, 10, or 20 Hz (5 ms pulse) or single 500 ms pulses with a power output at the tip of the connecting fiber of 12 mW @ 470 nm. After recording in baseline conditions mice were anesthetized using isoflurane (2% in O_2) perfused into the testing chamber at 1 LPM to test the effects of stimulating nAmb neurons under anesthesia. Atropine methyl nitrate (Cayman Chemicals, catalog # 9002272) dissolved in saline at 100 µg/mL was administered intraperitoneally to block muscarinic receptors after mice recovered from isoflurane anesthesia and then mice were re-tested 15 minutes after injection.

Voluntary Dive Training

Npy2r-Cre;Chat-Flp;dsHTB and C57Bl6j mice were trained to voluntarily dive underwater according to a protocol adapted from a previous publication (Hult et al., 2019). A diving pool was built from a 69 cm long x 38 cm wide x 10 cm high plastic tub. A channel was created in the center of the pool by affixing two 69 cm long x 0.32 cm wide x 10 cm high plexiglass strips with 2.5 cm perpendicular ledges 6 cm from the bottom, one third and two thirds of the way across

the length of the pool. These served as rails along which water-level barriers were placed to extend the length of the underwater dive. Squares of 10 cm x 0.6 cm x 10 cm plexiglass were used to construct walls around the starting end of the pool. To set up the diving enclosure for training, the two plexiglass strips were taped in place onto either end of the container and water was added to the tank to the desired level. Water temperatures were kept between 33 °C and 37 °C to prevent hypothermia and minimize stress. A raised platform was placed at the opposite end for the mouse to climb out of the water (escape platform). Small circles were drawn every 15 cm on the inside walls of the two plexiglass strips to help guide the mice while underwater. Additionally, a large "X" was drawn on the underwater portion of the platform for the same purpose. The diving enclosure was set up with the platform and thermometer and filled with water before every dive training session; and drained and cleaned after every session. A heat lamp was set up approximately 30 cm above the recovery cages to provide warmth after dive completion. At the start of each swim or dive, the mouse was taken from its home cage, placed at the starting end of the pool, allowed to swim across to the escape platform, and then removed from the pool and placed into its home cage under the warming lamp.

A 5-day progressive protocol for dive training mice was performed as follows. On Day 1 of dive training, mice were allowed 2 min to explore the pool with 1 cm of water. If a mouse touched the escape platform with all 4 paws within 2 min, they were immediately removed from the pool. If they failed to reach the escape platform, they were removed after 2 min. This was repeated 7 times. On Day 2 of dive training, mice were allowed to explore with the same criteria as in Day 1, for two trials. Then, water was added up to 3 cm and mice were allowed to wade through the water, for two trials. Water was added up to 5 cm, so the mice were unable to touch the bottom of the enclosure while swimming, for 7 trials. On Day 3, mice underwent a series of underwater dive trials of increasing distances: one trial of a 1 cm long dive; two trials of a 3 cm long dive; four trials of a 5 cm long dive; and six trials of a 6 cm long dive. On Day 4, mice underwent one trial each of 1 cm, 3 cm and 5 cm long dives, two trials of a 1cm long dive, and 5 trials of a 10 cm long dive. On Day 5, mice did one trial each of 1 cm, 3 cm and 5 cm long dives, two trials each of a 1 cm and a 10 cm long dive, and five trials of a 20 cm long dive. Dive repetitions were increased or decreased depending on each mouse's learning speed.

Electrocardiography

After dive training completion, mice underwent surgical implantation of electrocardiography (EKG) telemeters (Data Science International, DSI; ETA-F10) for wirelessly recording heart rate at rest and during diving. Each mouse was anesthetized with isoflurane and placed in dorsal recumbency on the auto-heated surgical table. The skin on the chest and upper abdomen was shaved, cleaned with alcohol and iodine, and 0.1mL of Nocita (long-lasting Bupivacaine, 13.3 mg/mL) was injected at the midline of the sternum, with the limbs loosely taped down. A 2 cm shallow, vertical inline incision was made along the sternum and, using blunt-tip hemostatic forceps, a subcutaneous pocket starting at the left caudal edge of the incision was created down the lateral flank. Once the pocket size was increased to ensure adequate fit for the probe, the pocket and the probe were rinsed with sterile saline. The device ID number was noted alongside the mouse ID and the probe inserted into the pocket with the leads oriented cranially (red lead on the left and white lead on the right). The leads were trimmed to the appropriate length to allow for placement in desired locations. The red lead was routed subcutaneously by blunt dissection to the left flank inferior to the underarm and secured with a 6.0 silk suture to the muscle. The white lead was routed subcutaneously across the torso to the upper right pectoralis major and secured with a 6.0 silk suture. Secure attachment of the probe was confirmed by slightly tugging on the leads. The incision was closed with 3 mouse wound clips and antibiotic ointment was applied. The wound clips were reapplied if dislodged by the mouse and subsequently removed 7-10 days later.

Diving Reflex Assay

For diving-induced *Fos* experiments, a total of 13 (7 female, 6 male) mice were trained according to the above protocol. Before training, mice were administered Fluorogold (FG; i.p. as described above) to label nAmb neurons. After 5-7 days of training, mice were randomly assigned into groups (voluntary dive or no dive). For voluntary diving, (4 female, 3 male mice) mice were introduced into the diving chamber filled with water and allowed to dive voluntarily to reach the platform. Upon reaching the platform, mice were given 10-15 sec rest before being returned to the opposite end of the apparatus to dive again. For 20-30 min mice completed 20 to 40 individual dives before being placed in a warmed recovery chamber for 20 min to allow time for *Fos* mRNA expression. As a control ('no dive'), mice were placed in the diving enclosure filled with 1 cm of water and allowed to explore for 30 min before being placed in a warmed recovery chamber for 20 min before perfusion.

Mice were deeply anesthetized with a mixture of ketamine (100 mg/kg) and dexmedetomidine (0.2 mg/kg) given i.p. and perfused transcardially with 4% paraformaldehyde, pH 7.4 in 100 mM phosphate buffers. Brains were removed and post-fixed in the same fixative for 12-24 hr at 4°C. Brains were sectioned (30-50 μm) on a vibratome (VT-1000S, Leica Biosystems, Deer Park, IL, USA), and sections were stored in cryoprotectant (30% ethylene glycol (v/v), 20% glycerol (v/v), 50% 100mM phosphate buffer, pH 7.4) at −20°C. Multiplex fluorescent in situ hybridization was performed using RNAscope (V1 kit, Advanced Cell Diagnostics, Newark, CA, USA). Probes for *Npy2r*, *Chat*, and *Fos*, and native fluorescence was used to identify Fluorogold+ cells. Serial 1-in-3 sections were washed in RNase(ribonuclease)-free phosphate buffered saline, mounted on charged slides, dried overnight, and processed according to the manufacturer's instructions. Immediately following the RNAscope procedure, sections were rinsed and then incubated in blocking solution for 10 min followed by incubation in primary at room temperature for 60 min, rinsed and incubated in secondary antibodies for 30 min, rinsed and then dried overnight before cover slipping. Slides were cover slipped with Prolong Gold antifade mounting media with DAPI (Thermo Fisher Scientific, catalog # P3693).

All nAmb neurons on one side of the brain between the spinal decussation and facial nucleus were counted. Only cells that contained FG fluorescence and stained for *Chat* RNA were included. Presence or absence of *Npy2r* and *Fos* RNA was determined for each FG+/*Chat*+ nAmb neuron. A cell was considered *Fos*+ if it contained >5 bright *Fos* puncta.

KEY RESOURCES TABLE

REAGENT or RESOURCE	SOURCE	IDENTIFIER
Antibodies		
Rabbit PGP9.5	Abcam	Cat # Ab108986; Lot # GR3371329-19
Goat anti-Tdtomato	Arigo Biolaboratories	Cat # Af449; Lot # ARG55724
Chicken PGP9.5	Thermo Fisher	Cat # PA1-46204; Lot # YE3918326A
Rabbit anti-RFP	Rockland	Reference # p/n 600-401-379; Lot # 48710

Goat anti-Chat	Sigma Aldrich	Cat # AB144P; Lot # 3491643
Donkey anti-goat 568	Invitrogen	Ref # A11057; Lot # 1975005
Donkey anti Rabbit 647	Invitrogen	Ref # A31573; Lot # 2083195
Donkey anti-chicken 647	Invitrogen	Ref # A21449; Lot # 2010133
Donkey anti Rabbit 594	Abcam	Ref # Ab96893; Lot # GR3276143-1
Donkey anti-Gt 647	Invitrogen	Ref # A21447; Lot # 2273668
Donkey anti-goat 488	Invitrogen	Ref # A11055; Lot: 1942238
Bacterial and virus strains		
AAV9-FLEX-tdTomato	AddGene	Plasmid # 28306
Chemicals, peptides, and recombinant proteins		
Fluorogold	Fluorochrome	Cat # Fluoro-gold; RRID: AB_2314408
TSA Plus Fluorescein Reagent	Akoya Biosciences	Cat # TS-000200
TSA Plus Cy3 Reagent	Akoya Biosciences	Cat # TS-000202
TSA Plus Cy5 Reagent	Akoya Biosciences	Cat # TS-000203
Critical commercial assays		
RNAscope Multiplex Fluorescent Reagent Kit V2	Advanced Cell Diagnostics	Cat # 323100
Deposited data		
Raw and processed single-nuclei RNA-seq data files	Gene Expression Omnibus (GEO)	TBD
Clustered single-nuclei RNA-seq data	Broad Single Cell Portal	TBD
Experimental models: Organisms/strains		
Mouse/Chat-IRES-Cre	Jackson Laboratory; Rossi et al., 2011	RRID: IMSR_JAX: 031661
Mouse/Phox2b-Flp	Jackson Laboratory; Hirsch et al., 2013	RRID: IMSR_JAX: 022407

Mouse/Crhr2-CreEGFP	Anthony et al., 2014	N/A
Mouse/Vipr2-IRES-Cre	Jackson Laboratory; Daigle et al., 2018	RRID: IMSR_JAX: 031332
Mouse/Chat-p2a-Flp	Gift of Brad Lowel	Coverdell *et al.,* 2022
Mouse/Npy2r-IRES-Cre	Chang *et al.* 2015	N/A
Mouse/Adcyap1-2A-Cre	Jackson Laboratory; Harris JA, et al. 2014	RRID: IMSR_JAX: 030155
Mouse/H2b-TRAP	Gift of Evan Rosen and Linus Tsai	RRID: IMSR_JAX: 029789
Mouse/CaTCh	Jackson Laboratory; Daigle et al., 2018	RRID: IMSR_JAX: 025109
Oligonucleotides		
Mm-Chat	Advanced Cell Diagnostics	Cat # 408731
Mm-Chat-C2	Advanced Cell Diagnostics	Cat # 408731-C2
Mm-Chat-C3	Advanced Cell Diagnostics	Cat # 410071-C3
Mm-Npy2r	Advanced Cell Diagnostics	Cat # 315951
Mm-Adcyap1	Advanced Cell Diagnostics	Cat # 405911
Mm-Adcyap1-C2	Advanced Cell Diagnostics	Cat # 405911-C2
Mm-Crhr2-C2	Advanced Cell Diagnostics	Cat # 413201-C2
Mm-Crhr2-C3	Advanced Cell Diagnostics	Cat # 413201-C3
Mm-Vipr2	Advanced Cell Diagnostics	Cat # 465391
Mm-Vipr2-C2	Advanced Cell Diagnostics	Cat # 465391-C2
Mm-CRE-C3	Advanced Cell Diagnostics	Cat # 312281-C3
Mm-Flp	Advanced Cell Diagnostics	Cat # 1157161-C1
Mm-Phox2b-C2	Advanced Cell Diagnostics	Cat # 407861-C2
Mm-Phox2b-C3	Advanced Cell Diagnostics	Cat # 407861-C3
Software and algorithms		

R	R version 4.1.2	https://www.r-project.org/; RRID: SCR_001905
Seurat v4.3.0	Stuart et al., 2019	https://github.com/satijalab/seurat/; RRID: SCR_007322
Seurat code used for cell clustering	Zenodo	TBD
Illustrator	Adobe	https://www.adobe.com; RRID: SCR_010279
Excel	Microsoft	https://www.microsoft.com/en-us/; RRID: SCR_016137
Mouse genome	10X Genomics	mm10-2020-A
bcl2fastq v2.20.0	Illumina	https://support.illumina.com/sequencing/sequencing_software/bcl2fastq-conversion-software.html; RRID: SCR_015058
Cellranger/5.0.0	Illumina	Cell Ranger (RRID:SCR_017344)

FIGURES

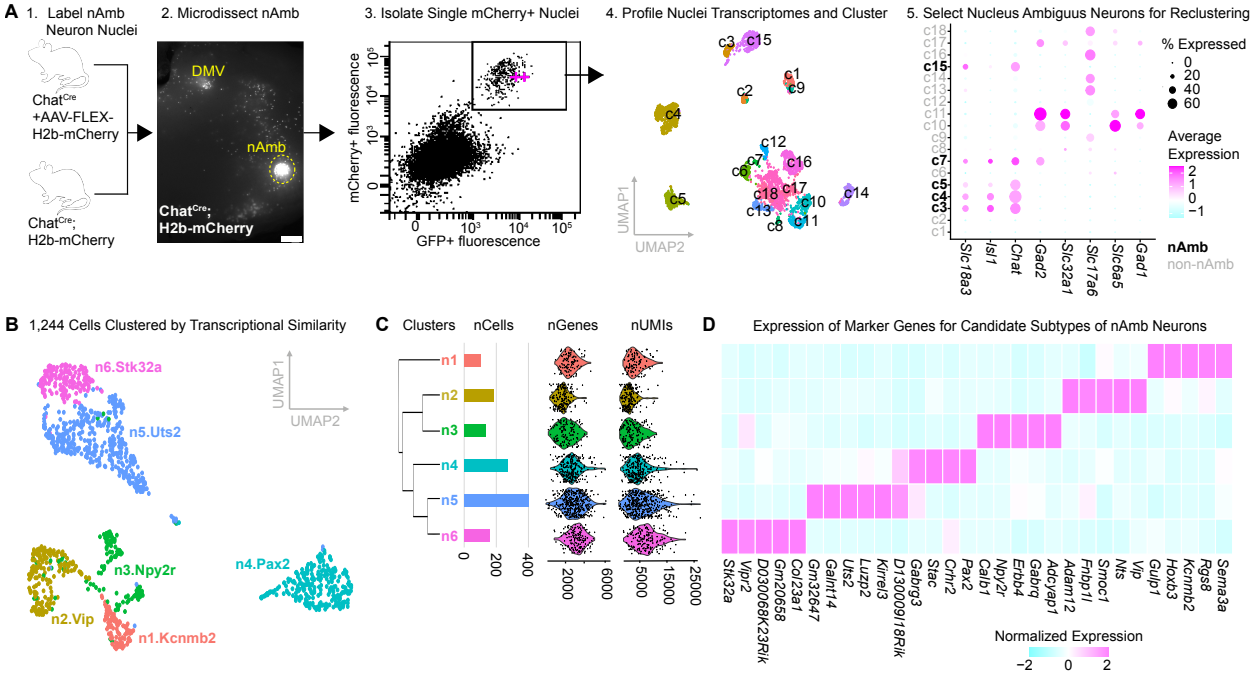

Figure 1: Molecular Classification of Nucleus Ambiguus Neurons

a. Schematic representation of the single-nuclei RNA-sequencing workflow. From left to right: labeling and isolation of nucleus ambiguus (nAmb) neurons using Chat-Cre;H2b-TRAP mice and Chat-Cre mice injected with a Cre-dependent H2b-mCherry AAV; uniform manifold approximation and projection (UMAP) of all neuronal clusters; dot plot of positive and negative marker genes used to identify nAmb neurons.

b. UMAP visualization of only nAmb neurons clustered by transcriptomic similarity.

c. From left to right: dendrogram illustrating relatedness of clusters; number of cells, genes and unique molecular identifiers (UMIs; ~unique RNA transcripts).

d. Selected candidate marker genes for each nAmb neuron cluster.

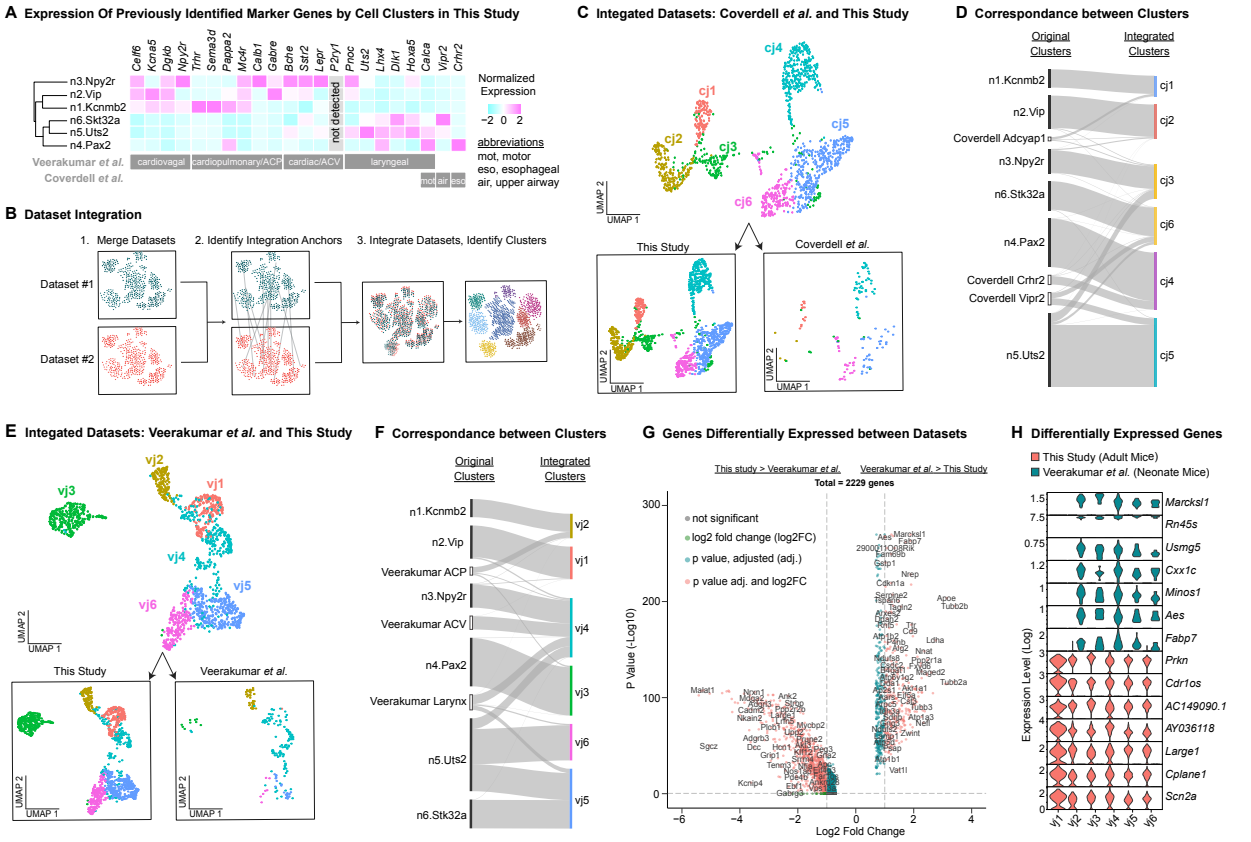

Figure 2: Integrated Analysis Predicts Functional Identities of Nucleus Ambiguus Neuron Subtypes

a. Marker genes from previous studies expressed by nAmb neuron clusters in our study.
b. Schematic of dataset integration. Figure panel created with Biorender.com.
c. UMAP after integrating nAmb neuron transcriptomes from Coverdell et al. (2022) and the present study.
d. For Coverdell et al. (2022) and the present study, a Sankey plot showing each cell's membership in the original and integrated cell clusters.
e. UMAP after integrating nAmb neuron transcriptomes from Veerakumar et al. (2022) and the present study.
f. For Veerakumar et al. (2022) and the present study, a Sankey plot showing each cell's membership in the original and integrated cell clusters.
g. Enhanced volcano plot showing differentially expressed genes between adult nAmb neurons of the present study and the neonatal nAmb neurons of Veerakumar et al. (2022).
h. Violin plot of selected genes differentially expressed between adult nAmb neurons of the present study and the neonatal nAmb neurons of Veerakumar et al. (2022).

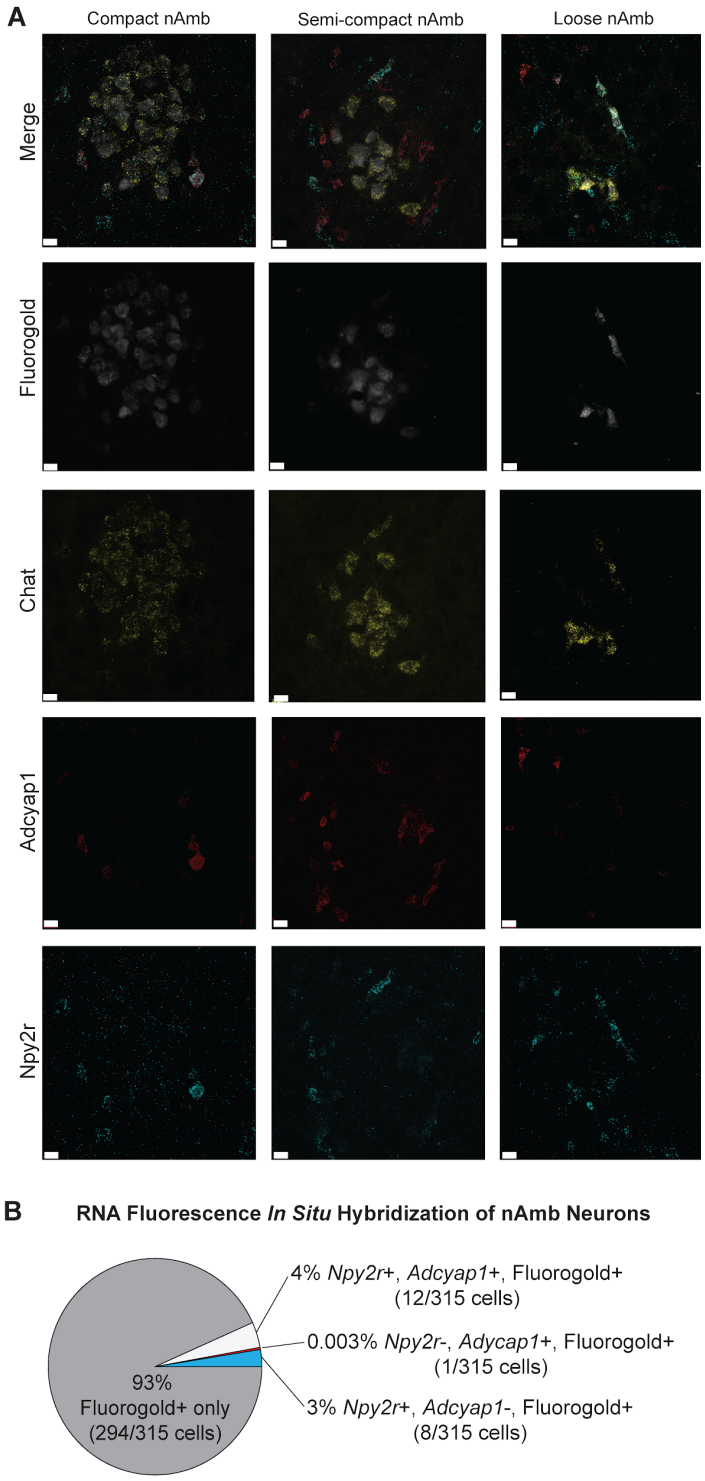

Figure 3: Partially Overlapping Populations of Nucleus Ambiguus Neurons Express *Npy2r* and *Adcyap1*

a. RNA FISH of *Npy2r* and *Adcyap1* in compact, semi-compact and loose nAmb. All nAmb vagal efferent neurons were labeled with RNA FISH for *Chat* and systemically administered Fluorogold. Scale bar, 20 µm.

b. Quantification of RNA FISH data (n=3 mice)

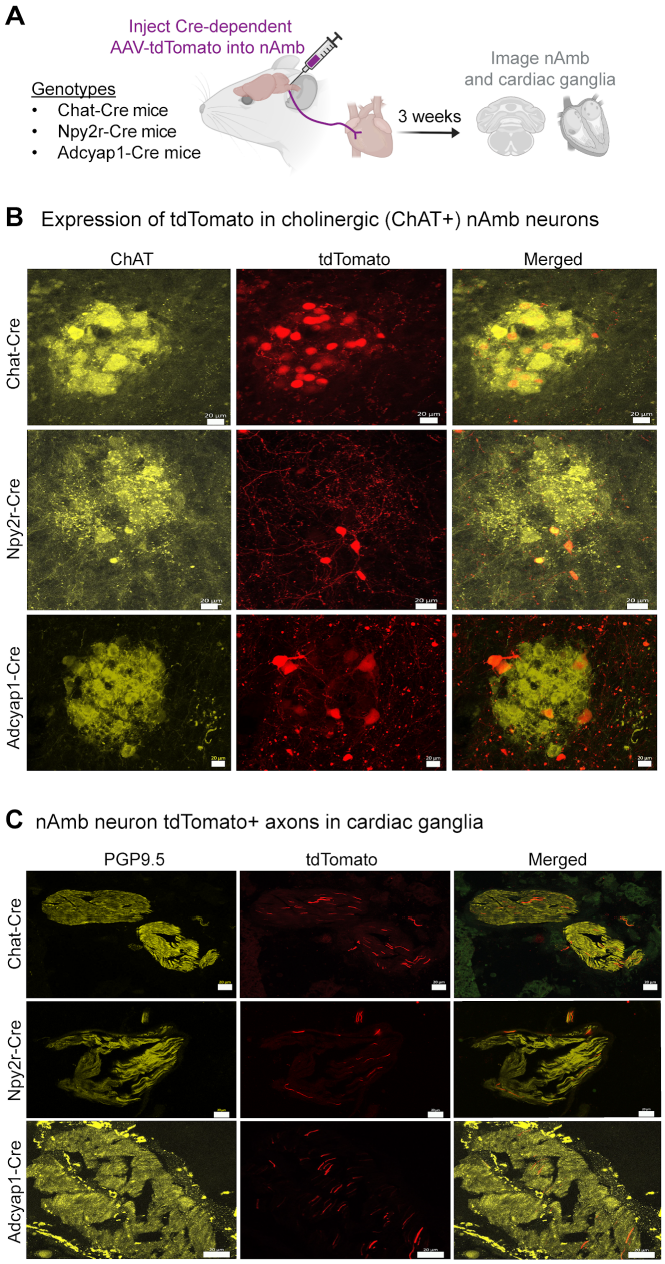

Figure 4: *Npy2r*- and *Adcyap1*-Expressing Nucleus Ambiguus Neurons Innervate Cardiac Ganglia

a. AAV-FLEX-tdTomato was injected into the right sided nAmb of Npy2r-Cre, Adcyap1-Cre,, and positive control Chat-Cre mice (n=3 mice per genotype) 3 weeks before collection of brain and heart tissue for immunofluorescence. Figure panel created with Biorender.com.

b. AAV Infected neuronal cell bodies in nAmb are labeled with red (tdTomato). Scale bar, 20 um.

c. tdTomato labeled axons of the infected neurons innervate the cardiac ganglia, , scale bar 20 um.

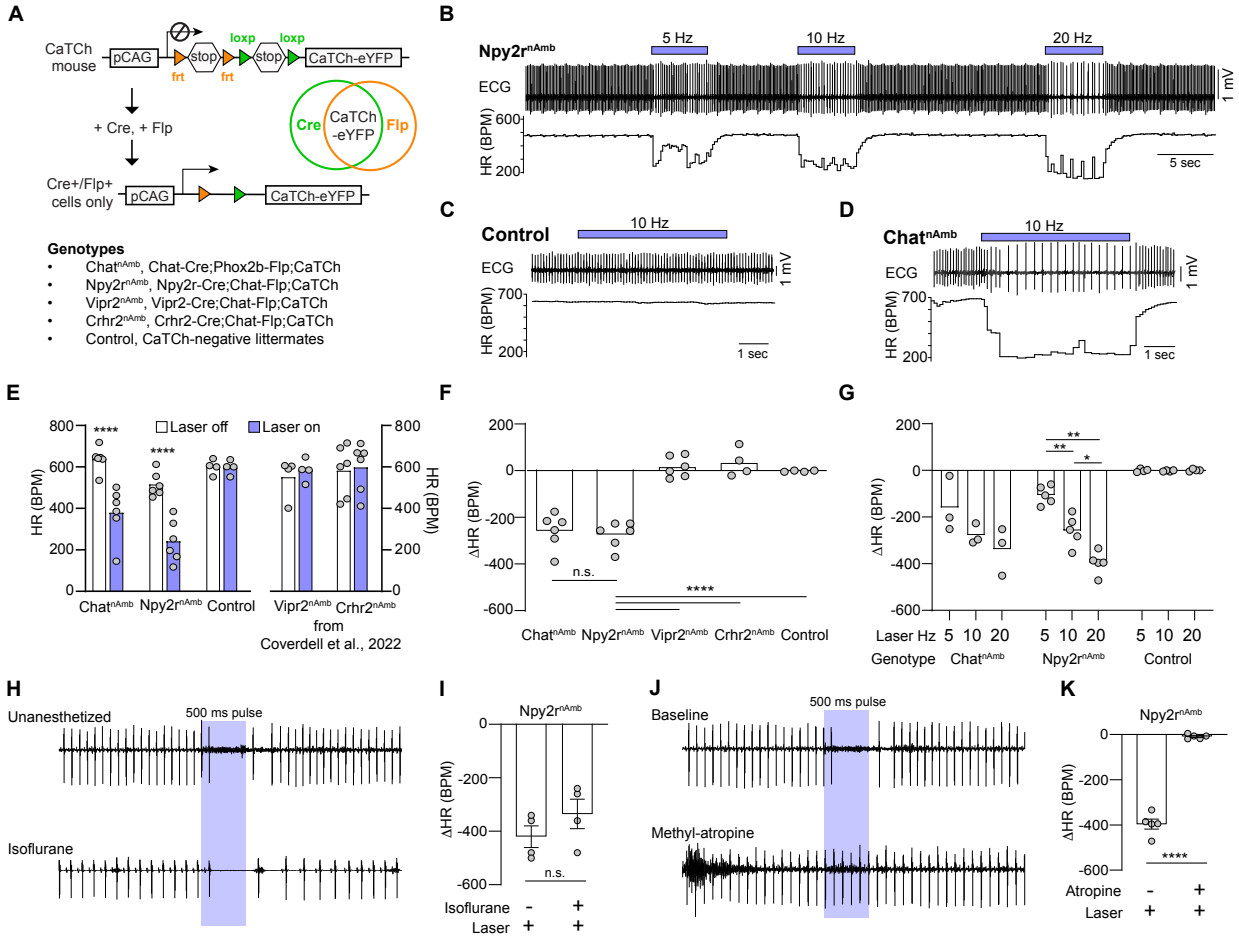

Figure 5: ***Activating*** **Npy2r-*Expressing Nucleus Ambiguus Neurons Reduces Heart Rate***

a. Strategy for intersectionally targeting CatCh-eYFP expression to nAmb neuron subtypes.

b. Experimental recording showing the effects of photostimulation of Npy2r^{nAmb} neurons at 3 different stimulus frequencies on electrocardiogram (ECG) and heart rate (HR). Note the rapid onset of bradycardia.

c. Experimental recording showing the lack of effect of photostimulation in negative controls that lack CatCh-eYFP expression.
d. Experimental recording showing the effect of photostimulation all nAmb neurons on HR
e. Grouped data for HR before and during photostimulation at 10 Hz of nAmb neuron subtypes. **** paired t-test for laser on and laser off condition for each group (t=12.07, df=5, p<0.0001 for all nAmb neurons; t=8.394, df=5, p=0.0004 for $Npy2r^{nAmb}$ neurons). Note that data for $Vipr2^{nAmb}$ neurons and $Crhr2^{nAmb}$ neurons is based on a previously published data set (Coverdell et al., 2022).
f. Grouped data for the change in HR with photostimulation at 10 Hz of nAmb neuron subtypes. There was no difference in the change in HR during photostimulation between $Chat^{nAmb}$ neurons and $Npy2r^{nAmb}$ neurons (p=0.97 by Tukey's multiple comparison post-test), and both these groups were significantly different from the remaining groups. Statistical comparison by one-way ANOVA, F(4, 21)=41.9, p<0.0001. **** p<0.0001 by Tukey's multiple comparison post-test.
g. The effect of photostimulation on HR was stimulation frequency-dependent when stimulating $Npy2r^{nAmb}$ neurons. Repeated measures one-way ANOVA F(2, 8) = 63.19, * p<0.05, ** p<0.01, ***p<0.001 by Tukey's multiple comparisons test
h. by Tukey's multiple comparisons test.
i. Experimental recording showing that bradycardia during photostimulation of $Npy2r^{nAmb}$ neurons was unaffected by isoflurane anesthesia (2% in oxygen).
j. Grouped data for the effect of photostimulation of $Npy2r^{nAmb}$ neurons at 20 Hz in unanesthetized and anesthetized conditions. Paired t-test, t=1.241, df=6, p=0.21
k. Experimental recording showing that the effect of photostimulation of $Npy2r^{nAmb}$ neurons on HR was blocked by systemic muscarinic receptor blockade with methyl-atropine (0.5 mg/kg, i.p.).
l. Grouped data for the effect of photostimulation of $Npy2r^{nAmb}$ neurons at 20 Hz after administration of saline or m-atropine in unanesthetized conditions. Paired t-test, t=15.11, df=4, p=0.0001.

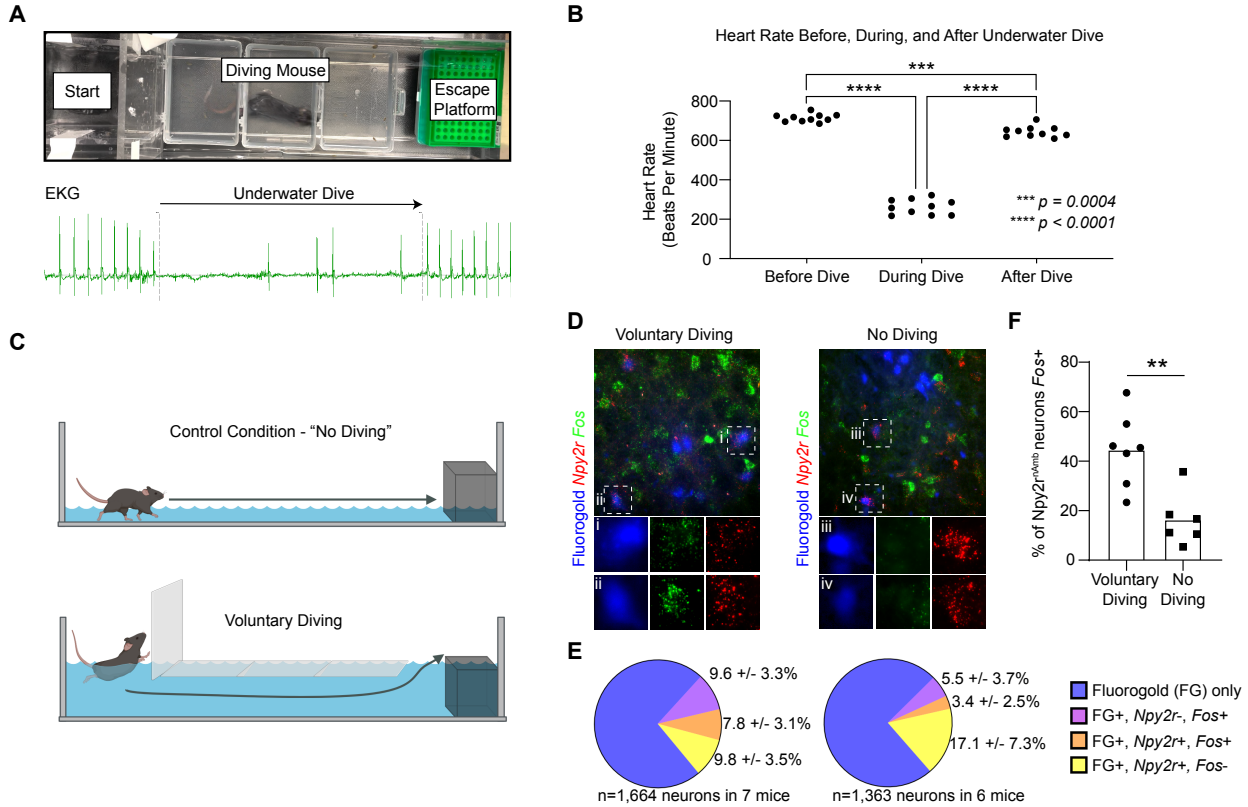

Figure 6: Voluntary Underwater Diving Activates Npy2r-Expressing Nucleus Ambiguus Neurons

A. Experimental set-up for voluntary diving assay (upper panel). EKG recorded during a voluntary dive (lower panel). EKG signal was collected using an implanted radio telemetry device.

B. Grouped data for heart rate during voluntary diving.

C. Experimental design to compare *Fos* expression in Npy2r nAmb neurons during voluntary diving and no-diving controls. Trained mice performed approximately 20-40 dives over a 20-30 min period followed by 30 min recovery period before perfusion for histology. Mice in the control condition performed no dives but were subjected to similar handling procedures. Figure panel created with Biorender.com.

D. RNA FISH of the immediate early gene *Fos* and the nAmb neuron subtype marker *Npy2r* after voluntary diving and control conditions. Systemically administered Fluorogold labels all nAmb vagal efferent neurons.

E. Quantification of *Fos* and *Npy2r* expression in Fluorogold+ nAmb neurons during voluntary diving (left) and control (right) conditions.

F. Comparison of the proportion of *Npy2r*+ nAmb neurons that expressed *Fos* in the voluntary diving and control condition. Unpaired t-test, t=3.915, df=11, p=0.0024

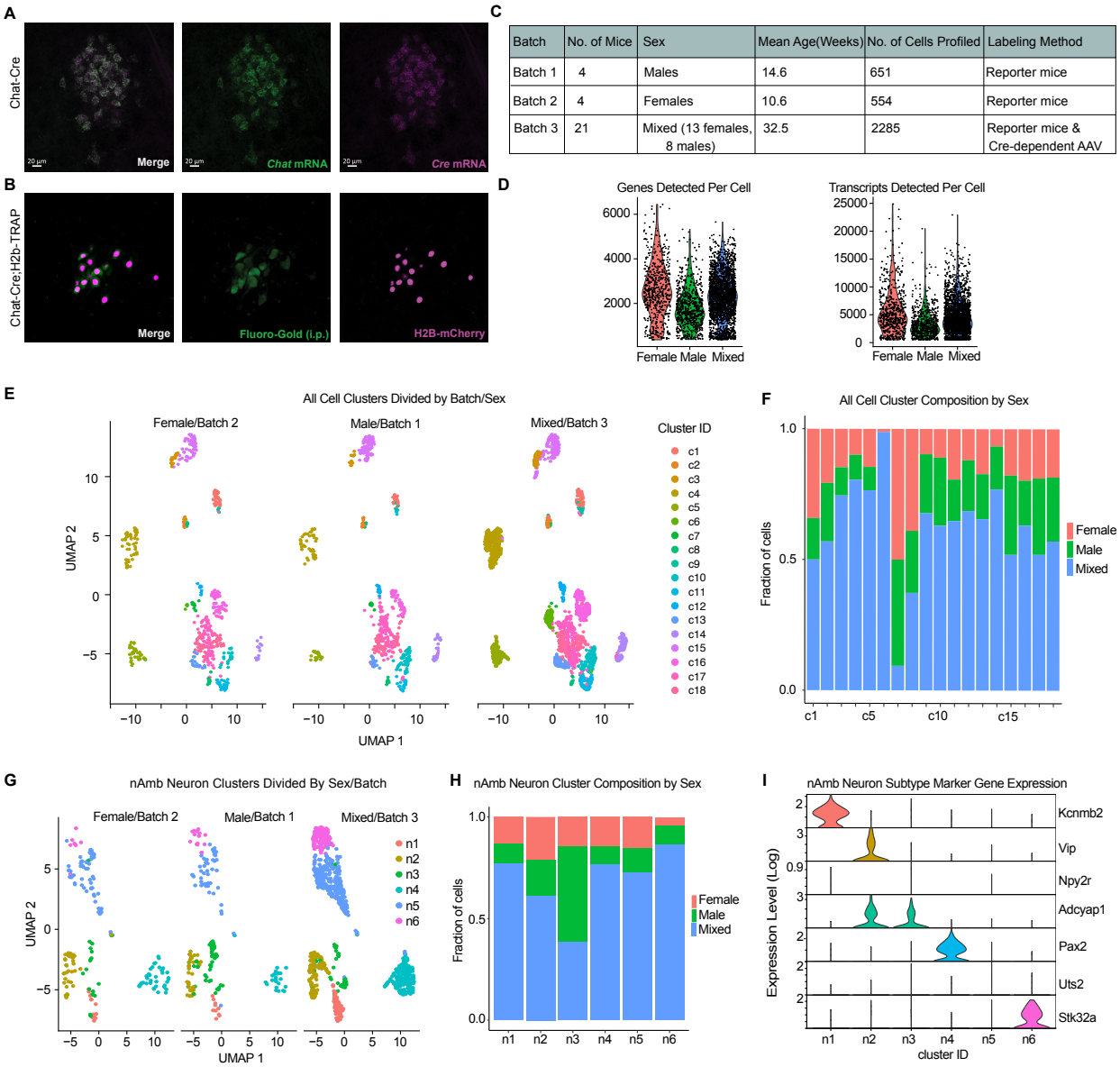

Batch	No. of Mice	Sex	Mean Age(Weeks)	No. of Cells Profiled	Labeling Method
Batch 1	4	Males	14.6	651	Reporter mice
Batch 2	4	Females	10.6	554	Reporter mice
Batch 3	21	Mixed (13 females, 8 males)	32.5	2285	Reporter mice & Cre-dependent AAV

Supplemental Figure 1: Quality Control of Mouse Lines and snRNA-seq Data

a. Validation of Chat-Cre mouse line by RNA fluorescent in situ hybridization (FISH) for *Chat* and *Cre*.

b. Chat-Cre;H2b-TRAP is expressed in nAmb vagal efferent neurons, which are labeled by systemic administration of Fluorogold.

c. Sample metadata for three sample batches of single-nuclei RNA-sequencing data.

d. Genes and unique transcripts (unique molecular identifiers, UMIs) detected per cell, by batch.

e. UMAP visualization of all neurons after batch integration.

f. Batch composition of each cell cluster in all-neuron UMAP.

g. UMAP visualization of only nAmb neurons after batch integration.

h. Batch composition of each cell cluster in nAmb-only UMAP.

i. Expression of candidate subtype marker genes in nAmb neuron clusters.

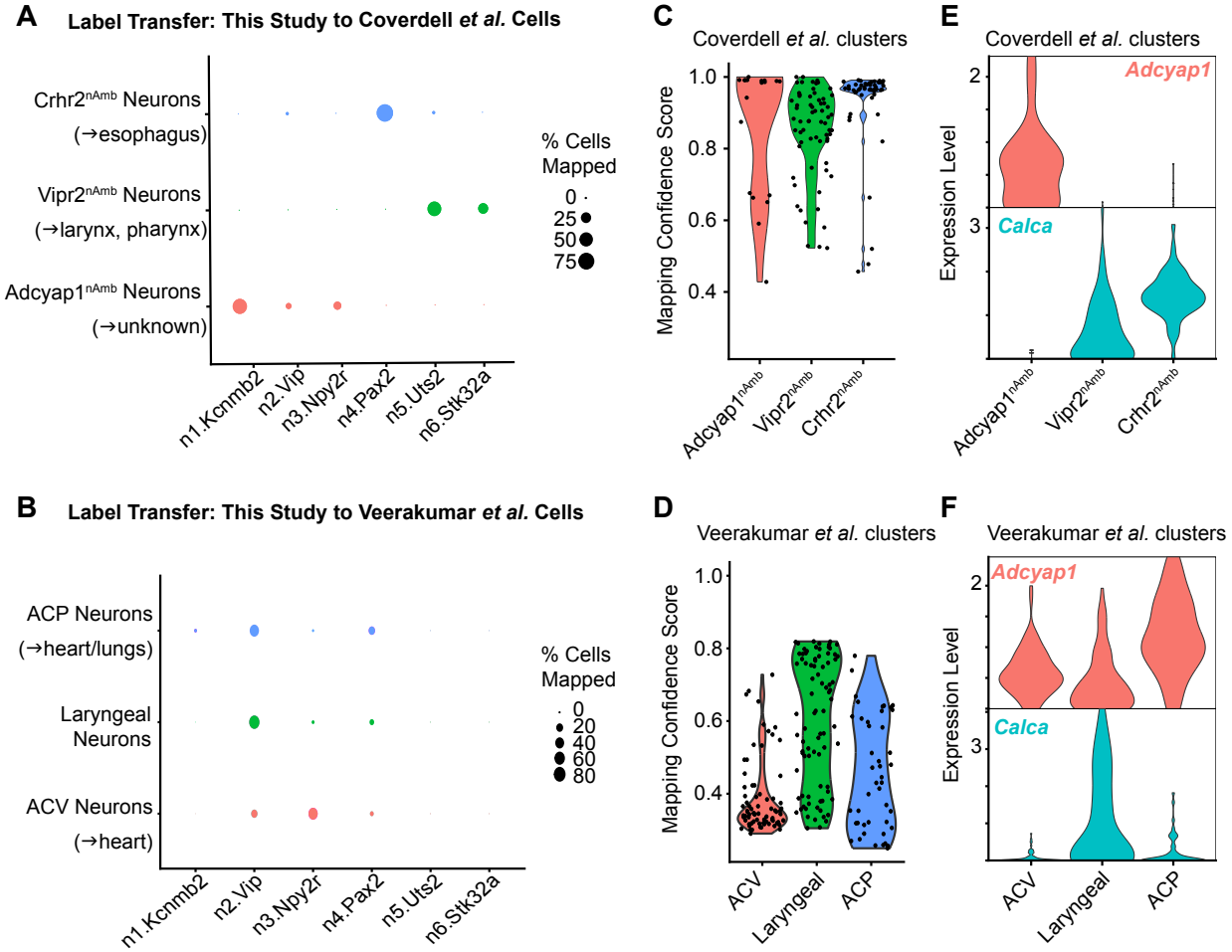

Supplemental Figure 2: Reference Query Mapping

a,b. Coverdell *et al.* (A) and Veerakumar *et. al* (B) query neuron clusters (y-axis) mapped onto the reference nAmb neuron clusters in the present study (x-axis).

c,d. Confidence of mapping of Coverdell et al. (c) and Veerakumar et al. (d) cells onto the nAmb neuron clusters of the current study.

e,f. Expression of *Adcyap1* and *Calca* by nAmb neuron clusters in Coverdell et al. (e) and Veerakumar et al. (f).

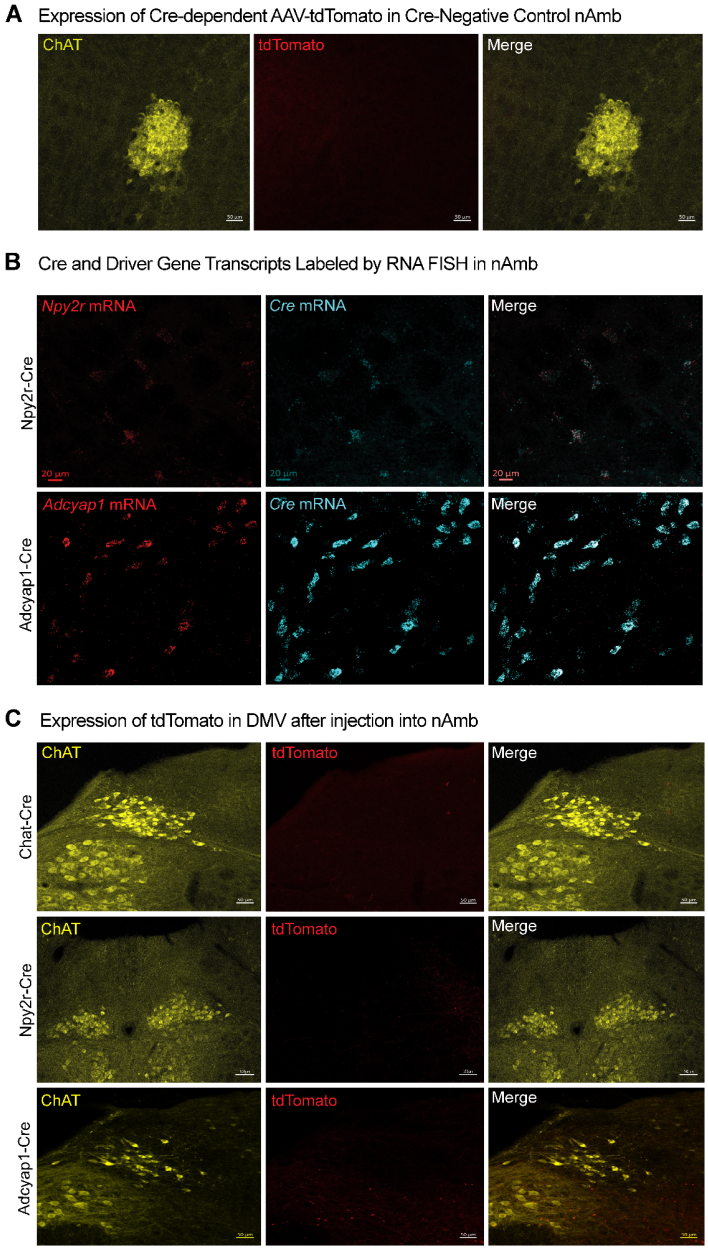

Supplemental Figure 3: Validation of AAV-DIO-tdTomato, Cre-Driver Mouse Lines, and nAmb Injection Specificity

a. tdTomato expression in C57Bl6/j nucleus ambiguus after AAV-DIO-tdTomato (negative control). Scale bar 50um.
b. RNA FISH validation of Cre specificity in Npy2r-Cre and Adcyap1-Cre mice (n=3 mice per line).
c. tdTomato expression in dorsal motor nucleus of the vagus (DMV) after AAV-DIO-tdTomato injection into nucleus ambiguus of Cre-expressing mouse lines (n=3 mice per genotype). Scale bar 50um.

REFERENCES

Alboni, P., Alboni, M., and Gianfranchi, L. (2011). Diving bradycardia: a mechanism of defence against hypoxic damage. J Cardiovasc Med (Hagerstown) *12*, 422-427.

Anderson, T.M., Garcia, A.J., 3rd, Baertsch, N.A., Pollak, J., Bloom, J.C., Wei, A.D., Rai, K.G., and Ramirez, J.M. (2016). A novel excitatory network for the control of breathing. Nature *536*, 76-80.

Armstrong, G., Martino, C., Rahman, G., Gonzalez, A., Vazquez-Baeza, Y., Mishne, G., and Knight, R. (2021). Uniform Manifold Approximation and Projection (UMAP) Reveals Composite Patterns and Resolves Visualization Artifacts in Microbiome Data. mSystems *6*, e0069121.

Bell, Z.W., Lovell, P., Mello, C.V., Yip, P.K., George, J.M., and Clayton, D.F. (2019). Urotensin-related gene transcripts mark developmental emergence of the male forebrain vocal control system in songbirds. Sci Rep *9*, 816.

Bieger, D., and Hopkins, D.A. (1987). Viscerotopic representation of the upper alimentary tract in the medulla oblongata in the rat: the nucleus ambiguus. The Journal of comparative neurology *262*, 546-562.

Butler, A., Hoffman, P., Smibert, P., Papalexi, E., and Satija, R. (2018). Integrating single-cell transcriptomic data across different conditions, technologies, and species. Nat Biotechnol *36*, 411-420.

Butler, P.J., and Jones, D.R. (1997). Physiology of diving of birds and mammals. Physiol Rev *77*, 837-899.

Calupca, M.A., Vizzard, M.A., and Parsons, R.L. (2000). Origin of pituitary adenylate cyclase-activating polypeptide (PACAP)-immunoreactive fibers innervating guinea pig parasympathetic cardiac ganglia. The Journal of comparative neurology *423*, 26-39.

Chang, R.B., Strochlic, D.E., Williams, E.K., Umans, B.D., and Liberles, S.D. (2015). Vagal Sensory Neuron Subtypes that Differentially Control Breathing. Cell *161*, 622-633.

Chang, Y., Lawson, L.J., Hancock, J.C., and Hoover, D.B. (2005). Pituitary adenylate cyclase-activating polypeptide: localization and differential influence on isolated hearts from rats and guinea pigs. Regulatory peptides *129*, 139-146.

Chen, H.I., and Chai, C.Y. (1976). Integration of the cardiovagal mechanism in the medulla oblongata of the cat. The American journal of physiology *231*, 454-461.

Cheng, Z., and Powley, T.L. (2000). Nucleus ambiguus projections to cardiac ganglia of rat atria: an anterograde tracing study. The Journal of comparative neurology *424*, 588-606.

Cheng, Z., Powley, T.L., Schwaber, J.S., and Doyle, F.J., 3rd (1999). Projections of the dorsal motor nucleus of the vagus to cardiac ganglia of rat atria: an anterograde tracing study. The Journal of comparative neurology *410*, 320-341.

Choate, J.K., Danson, E.J., Morris, J.F., and Paterson, D.J. (2001). Peripheral vagal control of heart rate is impaired in neuronal NOS knockout mice. Am J Physiol Heart Circ Physiol *281*, H2310-2317.

Coverdell, T.C., Abbott, S.B.G., and Campbell, J.N. (2024). Molecular cell types as functional units of the efferent vagus nerve. Semin Cell Dev Biol *156*, 210-218.

Coverdell, T.C., Abraham-Fan, R.J., Wu, C., Abbott, S.B.G., and Campbell, J.N. (2022). Genetic encoding of an esophageal motor circuit. Cell Rep *39*, 110962.

Dampney, R.A. (2016). Central neural control of the cardiovascular system: current perspectives. Adv Physiol Educ *40*, 283-296.

Feliciano, L., and Henning, R.J. (1998). Vagal nerve stimulation releases vasoactive intestinal peptide which significantly increases coronary artery blood flow. Cardiovasc Res *40*, 45-55.

Fryscak, T., Zenker, W., and Kantner, D. (1984). Afferent and efferent innervation of the rat esophagus. A tracing study with horseradish peroxidase and nuclear yellow. Anat Embryol (Berl) *170*, 63-70.

Fye, W.B. (2000). Profiles in cardiology. Ernst, Wilhelm, and Eduard Weber. Clin Cardiol *23*, 709-710.

Geis, G.S., Kozelka, J.W., and Wurster, R.D. (1981). Organization and reflex control of vagal cardiomotor neurons. J Auton Nerv Syst *3*, 437-450.

Geis, G.S., and Wurster, R.D. (1980a). Cardiac responses during stimulation of the dorsal motor nucleus and nucleus ambiguus in the cat. Circ Res *46*, 606-611.

Geis, G.S., and Wurster, R.D. (1980b). Horseradish peroxidase localization of cardiac vagal preganglionic somata. Brain research *182*, 19-30.

Goodwyn, E. (1786). Dissertatio medica de morteque submersorum investigandis. Department of Medicine, University of Edinburgh, Edinburgh.

Habib, N., Li, Y., Heidenreich, M., Swiech, L., Avraham-Davidi, I., Trombetta, J.J., Hession, C., Zhang, F., and Regev, A. (2016). Div-Seq: Single-nucleus RNA-Seq reveals dynamics of rare adult newborn neurons. Science *353*, 925-928.

Hao, Y., Hao, S., Andersen-Nissen, E., Mauck, W.M., 3rd, Zheng, S., Butler, A., Lee, M.J., Wilk, A.J., Darby, C., Zager, M.*, et al.* (2021). Integrated analysis of multimodal single-cell data. Cell *184*, 3573-3587 e3529.

Harris, J.A., Hirokawa, K.E., Sorensen, S.A., Gu, H., Mills, M., Ng, L.L., Bohn, P., Mortrud, M., Ouellette, B., Kidney, J.*, et al.* (2014). Anatomical characterization of Cre driver mice for neural circuit mapping and manipulation. Front Neural Circuits *8*, 76.

Harvey, R.D. (2012). Muscarinic receptor agonists and antagonists: effects on cardiovascular function. Handb Exp Pharmacol, 299-316.

Herring, N., Lokale, M.N., Danson, E.J., Heaton, D.A., and Paterson, D.J. (2008). Neuropeptide Y reduces acetylcholine release and vagal bradycardia via a Y2 receptor-mediated, protein kinase C-dependent pathway. J Mol Cell Cardiol *44*, 477-485.

Hirose, M., Furukawa, Y., Nagashima, Y., Lakhe, M., and Chiba, S. (1997). Pituitary adenylate cyclase-activating polypeptide-27 causes a biphasic chronotropic effect and atrial fibrillation in autonomically decentralized, anesthetized dogs. The Journal of pharmacology and experimental therapeutics *283*, 478-487.

Hirsch, M.R., d'Autreaux, F., Dymecki, S.M., Brunet, J.F., and Goridis, C. (2013). A Phox2b::FLPo transgenic mouse line suitable for intersectional genetics. Genesis *51*, 506-514.

Holstege, G., Graveland, G., Bijker-Biemond, C., and Schuddeboom, I. (1983). Location of motoneurons innervating soft palate, pharynx and upper esophagus. Anatomical evidence for a possible swallowing center in the pontine reticular formation. An HRP and autoradiographical tracing study. Brain Behav Evol *23*, 47-62.

Hult, E.M., Bingaman, M.J., and Swoap, S.J. (2019). A robust diving response in the laboratory mouse. J Comp Physiol B *189*, 685-692.

Kalia, M. (1981). Brain stem localization of vagal preganglionic neurons. J Auton Nerv Syst *3*, 451-481.

Lau, O.C., Shen, B., Wong, C.O., Tjong, Y.W., Lo, C.Y., Wang, H.C., Huang, Y., Yung, W.H., Chen, Y.C., Fung, M.L.*, et al.* (2016). TRPC5 channels participate in pressure-sensing in aortic baroreceptors. Nat Commun *7*, 11947.

Lawn, A.M. (1966). The localization, in the nucleus ambiguus of the rabbit, of the cells of origin of motor nerve fibers in the glossopharyngeal nerve and various branches of the vagus nerve by means of retrograde degeneration. The Journal of comparative neurology *127*, 293-306.

Levy, M.N. (1971). Sympathetic-parasympathetic interactions in the heart. Circ Res *29*, 437-445.

Li, Y.F., LaCroix, C., and Freeling, J. (2009). Specific subtypes of nicotinic cholinergic receptors involved in sympathetic and parasympathetic cardiovascular responses. Neurosci Lett *462*, 20-23.

Madisen, L., Garner, A.R., Shimaoka, D., Chuong, A.S., Klapoetke, N.C., Li, L., van der Bourg, A., Niino, Y., Egolf, L., Monetti, C.*, et al.* (2015). Transgenic mice for intersectional targeting of neural sensors and effectors with high specificity and performance. Neuron *85*, 942-958.

McAllen, R.M., and Spyer, K.M. (1976). The location of cardiac vagal preganglionic motoneurones in the medulla of the cat. J Physiol *258*, 187-204.

Merchenthaler, I. (1991). Neurons with access to the general circulation in the central nervous system of the rat: a retrograde tracing study with fluoro-gold. Neuroscience *44*, 655-662.

Muppidi, S., Gupta, P.K., and Vernino, S. (2011). Reversible right vagal neuropathy. Neurology *77*, 1577-1579.

Nosaka, S., Yamamoto, T., and Yasunaga, K. (1979). Localization of vagal cardioinhibitory preganglionic neurons with rat brain stem. The Journal of comparative neurology *186*, 79-92.

Nyegaard, M., Overgaard, M.T., Sondergaard, M.T., Vranas, M., Behr, E.R., Hildebrandt, L.L., Lund, J., Hedley, P.L., Camm, A.J., Wettrell, G.*, et al.* (2012). Mutations in calmodulin cause ventricular tachycardia and sudden cardiac death. Am J Hum Genet *91*, 703-712.

Ottaviani, M.M., and Macefield, V.G. (2022). Structure and Functions of the Vagus Nerve in Mammals. Compr Physiol *12*, 3989-4037.

Panneton, W.M. (2013). The mammalian diving response: an enigmatic reflex to preserve life? Physiology (Bethesda) *28*, 284-297.

Panneton, W.M., Anch, A.M., Panneton, W.M., and Gan, Q. (2014). Parasympathetic preganglionic cardiac motoneurons labeled after voluntary diving. Frontiers in Physiology *5*, 8.

Panneton, W.M., and Gan, Q. (2020). The Mammalian Diving Response: Inroads to Its Neural Control. Front Neurosci *14*, 524.

Reed, C. (1925). Effects of bilateral vagotomy on blood pressure. American Journal of Physiology-Legacy Content *74*, 61-69.

Reed, C., and Layman, J. (1930). Effects of bilateral vagotomy on blood pressure and heart rate. American Journal of Physiology-Legacy Content *92*, 275-281.

Richet, C. (1899). De la resistance des canards a l'asphyxie. J Physiol Pathol Gen *1*, 641-650.

Roh, H.C., Tsai, L.T., Lyubetskaya, A., Tenen, D., Kumari, M., and Rosen, E.D. (2017). Simultaneous Transcriptional and Epigenomic Profiling from Specific Cell Types within Heterogeneous Tissues In Vivo. Cell Rep *18*, 1048-1061.

Rossi, J., Balthasar, N., Olson, D., Scott, M., Berglund, E., Lee, C.E., Choi, M.J., Lauzon, D., Lowell, B.B., and Elmquist, J.K. (2011). Melanocortin-4 receptors expressed by cholinergic neurons regulate energy balance and glucose homeostasis. Cell metabolism *13*, 195-204.

Schmued, L.C., and Fallon, J.H. (1986). Fluoro-Gold: a new fluorescent retrograde axonal tracer with numerous unique properties. Brain research *377*, 147-154.

Sherman, D., Worrell, J.W., Cui, Y., and Feldman, J.L. (2015). Optogenetic perturbation of preBotzinger complex inhibitory neurons modulates respiratory pattern. Nature neuroscience *18*, 408-414.

Shuto, Y., Uchida, D., Onda, H., and Arimura, A. (1996). Ontogeny of pituitary adenylate cyclase activating polypeptide and its receptor mRNA in the mouse brain. Regulatory peptides *67*, 79-83.

Smith-White, M.A., Herzog, H., and Potter, E.K. (2002). Role of neuropeptide Y Y(2) receptors in modulation of cardiac parasympathetic neurotransmission. Regulatory peptides *103*, 105-111.

Standish, A., Enquist, L.W., and Schwaber, J.S. (1994). Innervation of the heart and its central medullary origin defined by viral tracing. Science *263*, 232-234.

Stuart, T., Butler, A., Hoffman, P., Hafemeister, C., Papalexi, E., Mauck, W.M., 3rd, Hao, Y., Stoeckius, M., Smibert, P., and Satija, R. (2019). Comprehensive Integration of Single-Cell Data. Cell *177*, 1888-1902 e1821.

Stuesse, S.L. (1982). Origins of cardiac vagal preganglionic fibers: a retrograde transport study. Brain research *236*, 15-25.

Sturrock, R.R. (1990). A comparison of age-related changes in neuron number in the dorsal motor nucleus of the vagus and the nucleus ambiguus of the mouse. J Anat *173*, 169-176.

Tanaka, I., Ezure, K., and Kondo, M. (2003). Distribution of glycine transporter 2 mRNA-containing neurons in relation to glutamic acid decarboxylase mRNA-containing neurons in rat medulla. Neurosci Res *47*, 139-151.

Thomas, M.R., and Calaresu, F.R. (1974). Localization and function of medullary sites mediating vagal bradycardia in the cat. The American journal of physiology *226*, 1344-1349.

Todd, W.D., Venner, A., Anaclet, C., Broadhurst, R.Y., De Luca, R., Bandaru, S.S., Issokson, L., Hablitz, L.M., Cravetchi, O., Arrigoni, E.*, et al.* (2020). Suprachiasmatic VIP neurons are required for normal circadian rhythmicity and comprised of molecularly distinct subpopulations. Nat Commun *11*, 4410.

Tompkins, J.D., Ardell, J.L., Hoover, D.B., and Parsons, R.L. (2007). Neurally released pituitary adenylate cyclase-activating polypeptide enhances guinea pig intrinsic cardiac neurone excitability. J Physiol *582*, 87-93.

Veerakumar, A., Yung, A.R., Liu, Y., and Krasnow, M.A. (2022). Molecularly defined circuits for cardiovascular and cardiopulmonary control. Nature *606*, 739-746.

Vega, J.L. (2017). Edmund Goodwyn and the first description of diving bradycardia. Journal of Applied Physiology *123*, 275-277.

Wang, F., Flanagan, J., Su, N., Wang, L.C., Bui, S., Nielson, A., Wu, X., Vo, H.T., Ma, X.J., and Luo, Y. (2012). RNAscope: a novel in situ RNA analysis platform for formalin-fixed, paraffin-embedded tissues. J Mol Diagn *14*, 22-29.

Weber, E.a.E.H. (1846). Experiences qui prouvent que les nerfs vague, stimulés par l'appariel de rotation galvano-magnetique, peuvent retarder et même arrêter le movement du coeur. Arch gen Med.

Zheng, G.X., Terry, J.M., Belgrader, P., Ryvkin, P., Bent, Z.W., Wilson, R., Ziraldo, S.B., Wheeler, T.D., McDermott, G.P., Zhu, J.*, et al.* (2017). Massively parallel digital transcriptional profiling of single cells. Nat Commun *8*, 14049.